The push and pull of abandoned channels: how floodplain processes and healing affect avulsion dynamics and alluvial landscape evolution in foreland basins

Harrison K. Martin and Douglas A. Edmonds

Department of Earth and Atmospheric Sciences, Indiana University,
Bloomington, IN 47408, USA

Correspondence: Harrison K. Martin (hkmartin@iu.edu)

Abstract. River avulsions are an important mechanism by which sediment is routed and emplaced in foreland basins. However, because avulsions occur infrequently, we lack observational data that might inform where, when, and why avulsions occur and these issues are instead often investigated by rule-based numerical models. These models have historically simplified or neglected the effects of abandoned channels on avulsion dynamics, even though fluvial megafans in foreland basins are characteristically covered in abandoned channels. Here, we investigate the pervasiveness of abandoned channels on modern fluvial megafan surfaces. Then, we present a physically based cellular model that parameterizes interactions between a single avulsing river and abandoned channels in a foreland basin setting. We investigate how abandoned channels affect avulsion setup, pathfinding, and landscape evolution. We demonstrate and discuss how the processes of abandoned channel inheritance and transient knickpoint propagation post-avulsion serve to shortcut the time necessary to set up successive avulsions. Then, we address the idea that abandoned channels can both repel and attract future pathfinding flows under different conditions. By measuring the distance between the mountain front and each avulsion over long (10^6 to 10^7 years) timescales, we show that increasing abandoned channel repulsion serves to push avulsions farther from the mountain front, while increasing attraction pulls avulsions proximally. Abandoned channels do not persist forever, and we test possible channel healing scenarios (deposition-only, erosion-only, and far-field-directed) and show that only the final scenario achieves dynamic equilibrium without completely filling accommodation space. We also observe megafan growth occurring via $\sim 100\,000$-year cycles of lobe switching but only in our runs that employ deposition-only or erosion-only healing modes. Finally, we highlight opportunities for future field work and remote sensing efforts to inform our understanding of the role that floodplain topography, including abandoned channels, plays on avulsion dynamics.

1 Introduction

Avulsions, the wholesale relocations of rivers into new positions on their floodplains, are a primary control on how water and sediment are routed through alluvial landscapes (Mackey and Bridge, 1995). The predominant conceptual model presents avulsions as requiring two necessary components: a setup and a triggering event that causes bank failure and avulsion (Slingerland and Smith, 2004). However, there is a lack of observational data on each of these necessary components because avulsions occur infrequently (Edmonds et al., 2016). Instead, avulsion dynamics are often explored using concept-driven numerical models. One such form is cellular models, which seek to reduce the system to the components necessary to reproduce a natural phenomenon (Jerolmack and Paola, 2007). For planform avulsion models, this

usually entails some description of sediment transport and deposition along an active channel and associated floodplain, and semi-heuristic rules for how avulsions are set up and used to initiate and pathfind (Hajek and Wolinsky, 2012). However, models have historically simplified or neglected the effect of abandoned channels on avulsion dynamics (Pelletier et al., 2005; Reitz et al., 2010). The relict topographic highs and lows associated with alluvial ridges and abandoned channels should affect both avulsion setup and avulsion pathfinding (Leeder, 1977; Allen, 1978; Jerolmack and Paola, 2007; Reitz et al., 2010). These effects could manifest as repulsion, if an approaching avulsing flow is restricted from entering an abandoned channel because of the topographic high formed by remnant levees, or attraction, if flow is routed along the topographic lows of former channel pathways (Edmonds et al., 2016).

The large, fan-shaped, low-relief fluvial megafans that exist where rivers leave lateral confinement and enter foreland basins are ideal locations to study the interaction between avulsions and abandoned channels (Fig. 1a; Leier et al., 2005; Weissmann et al., 2010). Fluvial megafans have some of the highest avulsion rates in the observational record (Valenza et al., 2020) and, in contrast to deltaic fans, have been qualitatively described as hosting abundant abandoned channels (e.g., Assine and Soares, 2004; Rossetti and Valeriano, 2007; Chakraborty et al., 2010; Bernal et al., 2011; Weissmann et al., 2013). However, we lack a detailed evaluation of the prevalence or distribution of this channelization, which is important to understand the degree to which avulsions may interact with abandoned channels.

In this paper, we present observational data on the channelization of fluvial megafan surfaces in alluvial foreland basin settings and we use these observations to motivate a physically based numerical model that parameterizes interactions between an avulsing river and abandoned channels in a subsiding basin. Our model implements tuneable abandoned channel dynamics that influence how abandoned channels affect pathfinding and are removed from the floodplain. Incorporating abandoned channel floodplain dynamics allows us to assess how abandoned channels affect where, when, and why avulsions occur. We demonstrate that abandoned channels, their interactions with future pathfinding flows, and the way they are removed from the floodplain are all important controls on avulsion locations, dynamics, and resulting foreland basin deposition and geomorphology that should be considered in future models and studies.

2   Background information

If abandoned channels are common features on floodplain surfaces, it is reasonable to expect that they should affect how avulsions find new pathways. Despite this, most previous models have assumed abandoned channels have no effect on future avulsion pathfinding (Leeder, 1977; Ratliff et al., 2018), or act as universal repulsors (Allen, 1978; Bridge and Leeder, 1979) or universal attractors (Sun et al., 2002; Jerolmack and Paola, 2007; Reitz et al., 2010). The reality seems to be somewhere in between these endmembers. Both remote sensing (e.g., Edmonds et al., 2016; Valenza et al., 2020) and stratigraphic (e.g., Mohrig et al., 2000; Chamberlin and Hajek, 2015, 2019) evidence suggests that avulsions commonly reoccupy former abandoned channel pathways. However, if abandoned channels retain the superelevation that caused avulsion and abandonment, then that superelevation would topographically repel later pathfinding events (Leeder, 1977; Allen, 1978).

Early alluvial stratigraphy models encoded the effects of abandoned channels on avulsion pathfinding differently. The pioneering Leeder (1977), Allen (1978), and Bridge and Leeder (1979) models created 2-D vertical slices of stratigraphy resulting from channel avulsion across a basin over time. These models required heuristic rules about where successive rivers would be emplaced, including choosing locations randomly (Leeder, 1977), according to lowest elevation (Bridge and Leeder, 1979), or randomly with additional elements of local abandoned channel repulsion (Allen, 1978). While their resulting stratigraphic sections were fairly insensitive to these differences (Hajek and Wolinsky, 2012), modern successors of these cross-section alluvial architecture models (e.g., Chamberlin and Hajek, 2015, 2019) have demonstrated that choosing different avulsion emplacement rules exerts a significant control on resulting stratigraphy. These rules position future channels along random (along a uniform distribution), compensational (at the lowest topographic elevation), or clustered (likelier to be closer to the previous channel position) distributions. While these rules prescribe the cross-basin location of successive channels without needing to resolve planform pathfinding, and the compensation rule contains an essence of repulsion as successive elevated abandoned alluvial ridges are left behind, it is unclear how flow routing due to abandoned channel repulsion or attraction further upstream affects or reflects each rule.

To avoid making explicit assumptions about channel emplacement, a parallel lineage of avulsion models resolve avulsion dynamics and pathfinding in a planform basin. These avulsion models necessarily require rules for hydrodynamics, sediment transport, and avulsion setup, initiation, pathfinding, and stabilization but allow for a more sophisticated interaction between avulsion pathfinding and floodplain topography (including abandoned channels) than can be resolved in cross-section models (Hajek and Wolinsky, 2012). Whenever these models incorporate topographic steepness (with or without random noise) into avulsion pathfinding, and do not instantly erase the topographic alterations made by abandoned channels on landscapes, pathfinding is controlled by abandoned channels (e.g., Mackey and Bridge, 1995; Coulthard et al., 2002; Sun et al., 2002; Jerolmack and Paola, 2007; Reitz et al., 2010). In addition to affecting avulsion dynamics, the rate at which these abandoned
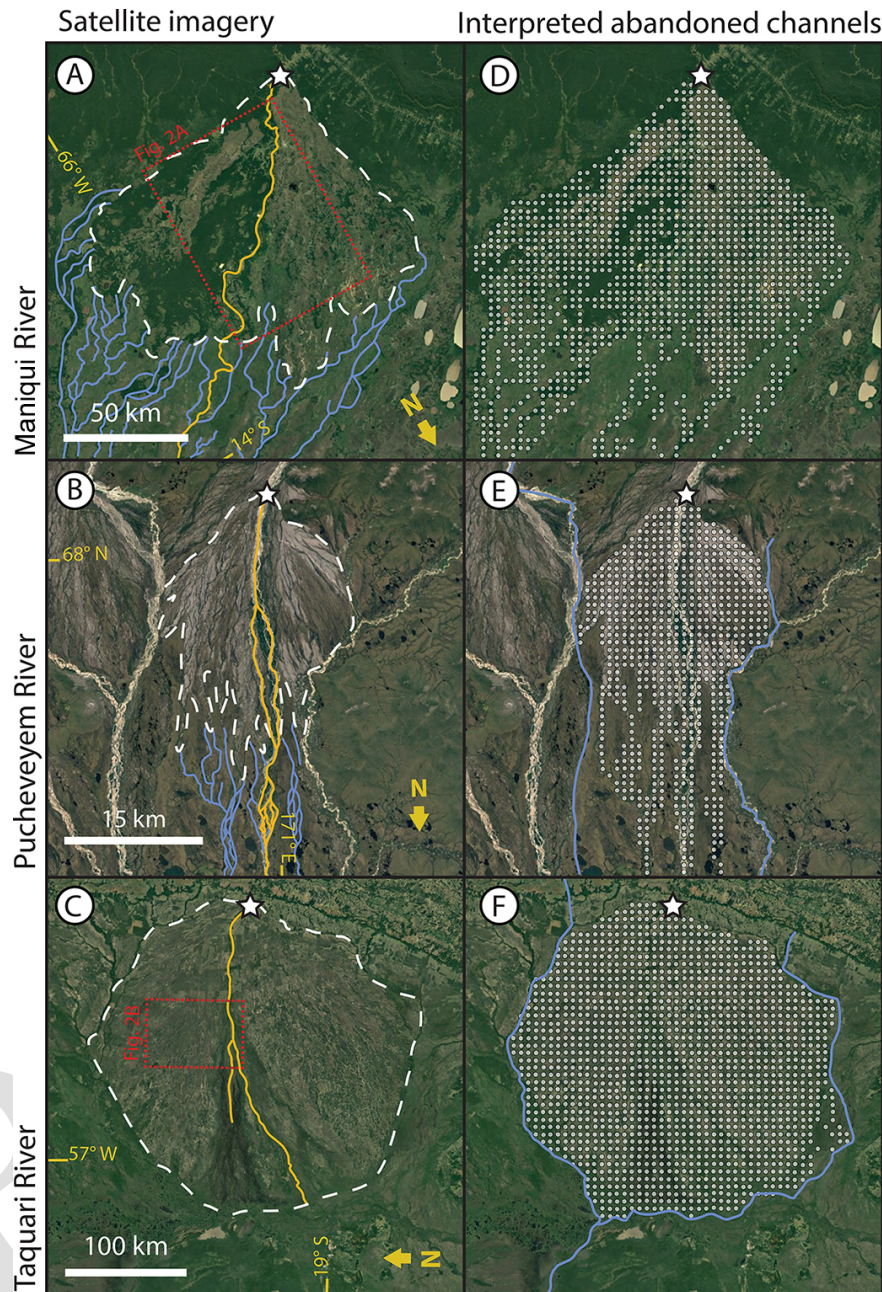
Figure 1. (a–c) Remote sensing images and **(d–f)** abandoned channel maps for three fluvial megafans. The fans are located along the Rápulo TS1 River in Bolivia **(a, d)**, the Pucheveyem River in Russia **(b, e)**, and the Taquari River in Brazil **(c, f)**. Note the downstream transition between distributive, densely channelized abandoned channel networks to tributive, sparsely channelized networks. Dashed white lines in panels **(a)**–**(c)** are interpreted megafan boundaries (see text for details), and white stars mark megafan apices. Blue lines in panels **(a)**–**(c)** show interpreted abandoned channel pathways outside of the megafan boundary. Solid gold lines show active channels. All satellite images are USGS/NASA Landsat/Copernicus, © Google Earth.

channels (and associated alluvial ridges and scours) are removed should affect avulsion pathfinding and hence landscape evolution. There are not many observations of abandoned channel healing rates, and those that exist are generally limited to sedimentation rates in oxbow lakes hydraulically connected to active channels (e.g., Cooper and Henry,

1989; Rowland et al., 2005; Wren et al., 2008; Kołaczek et al., 2017). As such, it is unclear in models whether to treat abandoned channels as healing instantly, persisting indefinitely, or some intermediary. As a broad classification, there are at least four assumptions that can describe the fate of these abandoned channels: (i) avulsed channels do not leave

behind abandoned channels on floodplains (instant healing; Ratliff et al., 2018, 2021), (ii) abandoned channels do not change after avulsion (no healing), (iii) abandoned channels are instantly healed after some fixed number of time steps (Reitz et al., 2010), or (iv) abandoned channels are healed gradually over time by adjusting their channel-base and/or levee-top elevations (Jerolmack and Paola, 2007). The first three assumptions do not allow abandoned channels to act as both repulsors and attractors, which is inconsistent with observations of avulsing rivers (Edmonds et al., 2016; Valenza et al., 2020). Further, the first assumption generates no abandoned channel topography on floodplains whatsoever.

Additionally, if one assumes that abandoned channels do heal, the mode of abandoned channel healing is unclear. While little is known about the constructive and destructive processes in action on floodplains, we can speculate on the evolution of abandoned channels using observations from both degradational and aggradational settings (Hartley et al., 2010b). During floods, overbank sediments can preferentially deposit in abandoned channel topographic lows (Wolman and Eiler, 1958; Schmudde, 1963; Bridge and Leeder, 1979; Lewis and Lewin, 1983; Farrell, 1987; Nanson and Croke, 1992; Tooth et al., 2002; Jerolmack and Paola, 2007; Toonen et al., 2012). This "bottom-up" healing, however, can be undone in some cases by scouring from future flooding events (Wolman and Leopold, 1957; Wolman and Eiler, 1958; Schmudde, 1963; Bridge and Leeder, 1979). The relative degree of levee erosion or deflation (something we call "top-down" healing) is unknown. Top-down healing is plausible if a combination of diffusive sediment transport, weathering, and fluvial erosion during floods erode or diffuse topographic highs on the floodplain (Hack and Goodlett, 1960; Burkham, 1972; Zwoliński, 1992; Gabet, 2000; Croke et al., 2013). High elevation on floodplains could be eroded during subsequent flood events or could conceivably be gradually diffused; while it is not clear whether diffusion should describe the evolution of alluvial floodplain topographic highs, biologic disturbance is often high (Richards et al., 2002; Steiger et al., 2005). Complicating matters, sediment deposition during overbank flows has also been observed atop flat or even positive floodplain topography, promoting self-sustaining topography that also hinders abandoned channel healing (Jahns, 1947; Wolman and Eiler, 1958; Schmudde, 1963; Nanson, 1980).

In summary, there are unanswered questions about the fates and rates of abandoned channel floodplain topography. There are virtually no data that describe how these landforms change through time once they are abandoned on the floodplain. This is an important knowledge gap because the primary mode of sediment transport and emplacement in this depositional environment is via alluvium deposited by and between avulsions. It is conceivable that the gross morphology of foreland basins and their deposits depends on the interaction between avulsing rivers and abandoned channels.

3 Observations of modern fluvial megafan surfaces

In order to motivate considering the importance of abandoned channels on avulsion dynamics, we must investigate the pervasiveness of abandoned channels in landscapes where avulsions are common. To do this, we created maps of abandoned channels on a non-exhaustive set of three megafans (Fig. 1) that represents a range of megafan sizes and settings with typical appearances (Hartley et al., 2010a; Weissmann et al., 2010). This set includes the well-studied Taquari megafan (e.g., Assine, 2005; Makaske et al., 2012; Zani et al., 2012). Following previous work (Rossetti and Valeriano, 2007; Bernal et al., 2011), we combine Google Earth, Landsat visual imagery, and bare-earth topography to identify abandoned channels on these megafans. For elevation data, we use the BEST (Bare-Earth SRTM Terrain) elevation model, which uses vegetation maps and satellite lidar to reveal bare-earth topography by correcting for vegetation elevations present in radar-derived topography (O'Loughlin et al., 2016; Moudrý et al., 2018). On top of each megafan, we overlaid a rasterized grid with square cells with dimensions that corresponded to roughly five channel widths, similar to the resolution of the cellular model that is described later. Within each cell we marked whether there was topographic or visual evidence of abandoned channels (Fig. 1d–f). Evidence of abandoned channels consisted of identified channelized features with long axes generally oriented toward the apex of the fan, with widths approximately equal to the active channels on the fan. Abandoned channels were usually visible in satellite imagery, but in areas with dense tree canopies, we looked for channel-like pathways delineated by differences in coloration against the adjacent floodplain. These differences result from the historical presence of an active channel (Bernal et al., 2011); abandoned channels may have coloration that is lighter (due to sediment emplacement; Valenza et al., 2020) or darker (due to increased vegetative density associated with additional standing or groundwater). Where possible, we used the topographic data in tandem with the visual data to confirm that a cell contained an abandoned channel.

3.1 Remote sensing results

These three fluvial megafans have abundant abandoned channels within their boundaries (Fig. 1). Megafan boundaries were drawn to encapsulate regions of positive relief and greater slope relative to the surrounding basin (dashed white lines, Fig. 1a–c). Within these boundaries, between 95 % (Rápulo) and > 99 % (Pucheveyem and Taquari) of cells on megafan surfaces contained interpreted abandoned channel features. Downstream of the megafan boundary there is a transition from distributive to tributive planform morphologies (Fig. 1a and b), wherever they are not bounded by topography or an axial river (Fig. 1c; see methodology of Hartley et al., 2010a). In contrast to other distributary fan systems

like alluvial fans or some deltas, within the fan we usually observed a single active channel with one or multiple threads and occasional bifurcation (Hartley et al., 2010a). This suggests that, rather than hosting many contemporaneous distributary channels, the distributive nature of megafans arises over time through repeated avulsions along a small number of active channels (Weissmann et al., 2010).

We observed that abandoned channels can be both topographic highs (associated with levees or alluvial ridges) and topographic lows (associated with abandoned channels that have not been fully filled in with sediment) relative to surrounding floodplains (Fig. 2). In some portions of the fan there were "internally drained" areas surrounded by topographic abandoned channel highs (Fig. 2a). These abandoned alluvial ridges were not necessarily spatially continuous in the downstream direction, often forming discontinuous ridges (Fig. 2; Rossetti and Valeriano, 2007). The topographic data were collected during an ongoing avulsion on the Taquari fan, and the avulsion location is immediately adjacent to a topographic low on its floodplain (Buehler et al., 2011). Multiple avulsions on the Rápulo megafan during the Landsat observation period have also initiated into local topographic lows adjacent to the channel (Edmonds et al., 2022).

3.2 Megafan floodplain topography discussion

The degree of floodplain channelization observed and interpreted on megafan surfaces in Figs. 1 and 2 compares well to the model results of Jerolmack and Paola (2007) and Reitz et al. (2010), and suggests that most avulsions should interact with abandoned channels. Following this, we envision at least two aspects of avulsion dynamics that can be influenced by the presence of abandoned channels and can be easily incorporated into a model.

Avulsion setup and initiation

The most common conception of avulsion setup is superelevation, whereby in-channel deposition outpaces deposition in the surrounding floodplain, leading to a perched channel that transports water and sediment less efficiently than some novel path on the floodplain (Bryant et al., 1995; Slingerland and Smith, 2004). On a flat, featureless floodplain where subsidence is uniform along strike, the time to achieve superelevation (T_A, years) for some arbitrary point along a river is commonly (e.g., Jerolmack and Mohrig, 2007; Jerolmack, 2009; Martin et al., 2009; Reitz et al., 2010; Moodie et al., 2019) approximated as

$$T_A = \frac{\beta \cdot h_{chan}}{A_{chan} - A_{fp,tot}}, \tag{1}$$

where β is a non-dimensional channel depth fraction (generally assumed to be 0.5–1.0; Mohrig et al., 2000), h_{chan} is the channel depth (meters) at a particular point in the river,
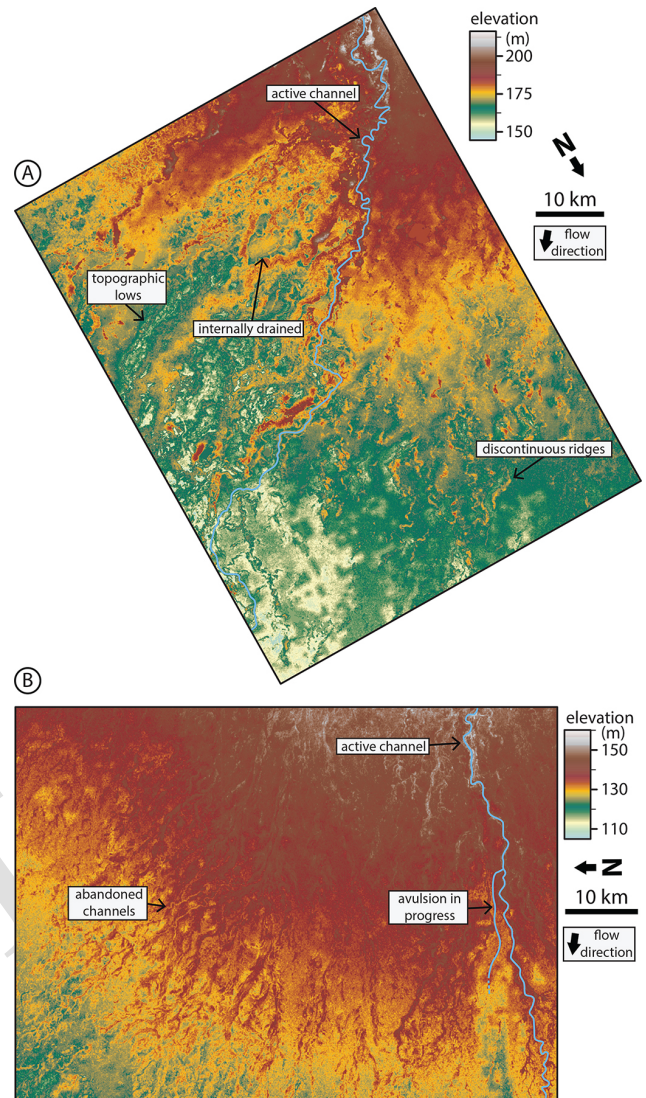
Figure 2. Bare-earth digital elevation models (O'Loughlin et al., 2016) of floodplain topography on the Rápulo **(a)** and Taquari **(b)** megafans. Locations are shown in Fig. 1. Floodplains are densely channelized by abandoned channels with visible topographic highs and lows corresponding to levees or alluvial ridges and channel beds, respectively. Note the presence of discontinuous alluvial ridges. Also note that the color bar is not perceptually uniform, meaning that small changes in certain elevation ranges are highlighted more drastically than others; this is done to emphasize low-relief features relative to the overall fan slope.

A_{chan} is the in-channel-bed aggradation rate (meters per year), and $A_{fp,tot}$ is the total floodplain aggradation rate (meters per year). Conceptually, this superelevation timescale is equal to the time necessary for the channel bed to aggrade some specified fraction of a channel depth (Fig. 3a).

Abandoned channels on the floodplain can short-circuit this timescale by reducing the amount of aggradation needed to superelevate (Fig. 3a). If an abandoned channel is close to
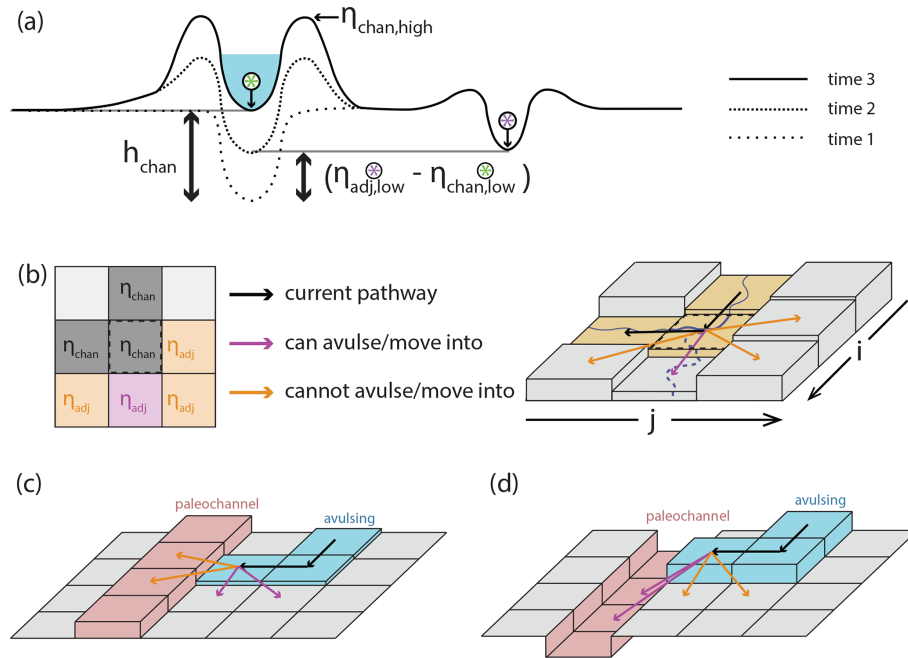
Figure 3. (a) Conceptual understanding of avulsion setup by superelevation and how the magnitude of in-channel aggradation necessary to achieve aggradation (black bidirectional arrows) differs if abandoned channels are ignored (left of active channel; Eq. 1) or considered (right of active channel; Eq. 2). **(b)** Representation of avulsion setup by superelevation in a 2-D cellular setting that considers adjacent elevations. Cells in the left panel are marked as η_{adj} if they are adjacent to the center cell, highlighted by the dashed black line in the left and right panels. In this case, the cell is superelevated and enjoys a gradient advantage toward one cell (immediately down domain) and can thus avulse into this cell. The subscript "low" applies to all labeled cells but is omitted for legibility. Model representation of **(c)** abandoned channel repulsion and **(d)** attraction.

the active one, then this should encourage avulsion because during high flow there would be a steep water surface gradient that would cause erosion of the intervening levee and reroute the flow. This requires that the abandoned channel is roughly the same size as the active one and that it is close enough to increase the water surface gradient. What constitutes "close enough" is unknown, though the Taquari avulsion is observed to proceed into an adjacent topographic low ($\sim 1\,\mathrm{km}$ from the parent channel; Fig. 2b), as are repeated avulsions along the Rápulo river (Edmonds et al., 2022). In effect, the lower elevation of the abandoned channel bed relative to its surrounding floodplain reduces the amount of aggradation needed for superelevation. We can thus rewrite the superelevation timescale of Eq. (1) as

$$T_{\mathrm{A}} = \frac{\beta \cdot \left(\eta_{\mathrm{adj,low}} - \eta_{\mathrm{chan,low}}\right)}{A_{\mathrm{chan}} - A_{\mathrm{fp,tot}}}, \text{ for } \eta_{\mathrm{adj,low}} > \eta_{\mathrm{chan,low}}, \quad (2)$$

where $\eta_{\mathrm{chan,low}}$ and $\eta_{\mathrm{adj,low}}$ represent the elevations (meters) of the active channel bed and the area adjacent to the channel, respectively (Fig. 3a and b). This adjacent elevation can vary based on the topography adjacent to the channel. For example, if there is an abandoned channel bed that is inset into the surrounding floodplain adjacent to the river, then the active channel becomes superelevated relative to the abandoned channel when $\eta_{\mathrm{chan,low}} = \eta_{\mathrm{adj,low}}$. When the difference of

$\eta_{\mathrm{adj,low}} - \eta_{\mathrm{chan,low}}$ is less than h_{chan} (see Fig. 3a), Eq. (2) will result in a shorter avulsion setup timescale than would be expected for a featureless floodplain (Eq. 1; Mohrig et al., 2000). Even though this is a simple amendment to Eq. (1), as we show later it has important effects on avulsion timing and location.

Channel reoccupation could also shorten superelevation timescales. Given the density of channels we observed on megafans (Figs. 1 and 2), and observations from the stratigraphic and remote sensing records, it seems that reoccupation must be common (e.g., Mohrig et al., 2000; Chamberlin and Hajek, 2015, 2019; Valenza et al., 2020). When active channels avulse, any previous aggradation downstream of the avulsion locus is not immediately destroyed. Instead, if these channels are later reoccupied, and had not been completely scoured out in the interim, then Eq. (2) allows for superelevation to be inherited. In these two ways, abandoned channels can cause rivers to have avulsion setup timescales that are much less than via relative aggradation alone as embodied in Eq. (1).

4 Model conception and implementation

4.1 Model overview and routine

The prevalent channelization of fluvial megafan surfaces led us to consider how abandoned channels may affect avulsion dynamics and landscape evolution in foreland basin settings. To test these effects, we created a physically based cellular model of an evolving alluvial landscape with parameterized and tuneable abandoned channel dynamics ("RiverWalk"; Martin and Edmonds, 2021). Our model is intentionally simplified as much as possible while retaining the ability to recreate the essential features of fluvial megafans in foreland basins (Bokulich, 2013). As a brief conceptual overview, our model consists of a single river exiting a mountain front and transporting water and sediment at some fixed rates. As it enters a foreland basin, relative subsidence (high near the mountain front, decreasing linearly into the basin) causes sediment to be deposited preferentially near the mountain front. This leads to river avulsion via superelevation, and over time these avulsions construct a radially oriented fan through the emplacement of channels that individually aggrade before abandonment. In our model, these abandoned channels can affect avulsion dynamics. For simplicity, we ignore the impacts of other rivers or fans and of any other mountain-front processes that may advect sediment into the basin. The model is generally insensitive to small changes in most non-experimental parameters (Sect. 6.1).

The model routine operates as follows; more details on individual components are provided in Tables 1 and 2 and in the sections that follow. We paired a 1-D diffusive channel-bed-elevation model (Paola et al., 1992) that describes how elevation in a river channel diffuses due to sediment transport with a rectangular, 2-D cellular computational domain of 150 km per side that describes the floodplain and surrounding basin. Following Jerolmack and Paola (2007), each cell has a low (channel-bed) and high (levee or alluvial ridge) elevation. The simulation initializes by assuming the channel takes a straight path to the bottom of the domain (Table 1). The 1-D sediment transport model is calculated to equilibrium along this path (Table 1). This profile is then used to initialize floodplain cells by setting the elevation of every floodplain cell equal to the equilibrium elevation an equal distance from the mountain front along this path. This creates an underfed basin because nearly all subsequent river paths will be longer than a straight line, which causes aggradation and avulsion.

After the first avulsion, a new river pathway is established within a single time step from the avulsion point (Sect. 4.3.1) and is set one channel depth below the surface. The pathway is selected via steepness-weighted random walk to any point along the bottom boundary of the domain (Sect. 4.3.1), and all floodplain cells along this path are converted to active channel cells (Sect. 4.3). The time step increments and the elevations of each cell along the new pathway are tran-

siently diffused to represent river adjustment (Sect. 4.3). At the upstream boundary of the diffusion model, water and sediment come in at a fixed rate so that the surface slope does not change (Table 2), and at the downstream boundary the channel-bed elevation is fixed at 0 m. Diffusion continues until an avulsion trigger (with a fixed probability at each time step) occurs and avulsion criteria (superelevation and gradient advantage) are satisfied for at least one active channel cell (Sect. 4.3.1). The avulsion location is randomly selected from among viable cells and pathfinding proceeds as before, but now the river can be repelled or attracted (i.e., captured) by abandoned channels. Pathfinding stops when the avulsion is successful and encounters the bottom boundary, or when the avulsion fails after becoming terminally trapped (Sect. 4.3.1). In both situations, the time step is incremented, but in the successful case any active channel cells that are no longer occupied become abandoned channel cells, and in the failure case the domain is restored to its pre-avulsion state.

In all future time steps, after updating the 2-D landscape and before checking for avulsion triggers, floodplain and abandoned channel processes routines are executed. First, cells experience subsidence at a rate that decreases away from the mountain front (representing a foreland basin) and overbank floodplain deposition that varies with distance from the mountain front but not with distance from the channel (Sect. 4.3.2). Next, abandoned channels are healed by a steady-rate topographic adjustment function until they reach a specified healing endpoint (Sect. 4.3.2). Finally, any abandoned channel cells with less than 25 % of a mean channel depth in remnant relief are converted to floodplain cells (Sect. 4.3).

4.2 1-D diffusive channel-bed elevation model

The 1-D model has a variable length that is equal to that of the planform river pathway established in the 2-D model. We used transient diffusion to model channel-bed elevation changes along this pathway that would occur from sediment transport (Paola et al., 1992):

$$\sigma + \frac{\partial \eta_{\text{chan,low}}}{\partial t} = \frac{\partial}{\partial x}\left(v\frac{\partial \eta_{\text{chan,low}}}{\partial x}\right), v = -\frac{8qA\sqrt{c_{\text{f}}}}{C_0(S-1)}, \quad (3)$$

where t is time (years), x is space (meters), v is diffusivity (square meters per year), q is normalized water discharge per unit basin width (square meters per year), A is a non-dimensional constant set to 1, c_{f} is a dimensionless drag coefficient, C_0 is bed sediment concentration, and S is sediment specific gravity ($\frac{\rho_{\text{sediment}}-\rho_{\text{water}}}{\rho_{\text{water}}}$, non-dimensional; Table 2). We used the Crank–Nicolson solution scheme to solve this equation. This scheme is second order, implicit in time, and unconditionally numerically stable for diffusion partial differential equations (Slingerland and Kump, 2011). Treating diffusion of the bed surface transiently (rather than bringing the river completely to equilibrium between each time step;

Table 1. Cellular model parameters. Values for parameters were chosen to be representative of rivers commonly found atop megafans in mountain-front regions, including those seen in Fig. 1.

Parameter	Value
Time step	10 year
Grid dimensions	301 cells × 301 cells
Cell size	500 m × 500 m
Random walk weights	In descending order of steepness: 40 %, 27.5 %, 17.5 %, 10 %, and 5 %
Minimum superelevation (β *sensu* Mohrig et al., 2000.)	Channel base equal to neighboring floodplain cell ($\beta = 1$)
Overbank aggradation (base rate; $A_{\text{fp,base}}$)	Upstream boundary: $2 \times 10^{-7} \, \text{m yr}^{-1}$ Downstream boundary: $5 \times 10^{-6} \, \text{m yr}^{-1}$
Subsidence rate (linearly interpolated; σ)	Upstream boundary: $1 \times 10^{-5} \, \text{m yr}^{-1}$ Downstream boundary: $5 \times 10^{-6} \, \text{m yr}^{-1}$
Initialization length	Variable; set such that initial apex elevation is $\sim$ 5 %–10 % less than final apex elevation; see Table 3

Table 2. Sediment diffusion calculation parameters.

Parameter	Value
Initial specific discharge (apex)	$1.9 \times 10^5 \, \text{m}^2 \, \text{yr}^{-1}$
Incoming sediment supply	$400 \, \text{m}^3 \, \text{yr}^{-1}$
Basin width (for discharge calculation)	$5 \times 10^4 \, \text{m}$
Coefficient A	1.00
Non-dimensional coefficient of friction	0.01
C_0	0.7
S	1.65
ρ_{sediment}	$2.65 \times 10^3 \, \text{kg m}^{-3}$
ρ_{water}	$1.00 \times 10^3 \, \text{kg m}^{-3}$

cf. Jerolmack and Paola, 2007) allows for local aggradation or incision to occur on channel profiles out of equilibrium.

Our experimental design necessitated using non-dimensional repulsion and attraction factors that are normalized to channel depths. As such, it was necessary to determine channel depth (h_{chan}) for each active channel cell. We solved for this at every active channel cell once per time step following Paola et al. (1992; Table 2). This method allows depth to vary as a function of local slope. Immediately after avulsion, slope variations along channels can be extreme. These extreme variations in slope create unrealistic variations in depth over short distances. As such, when solving for channel depth, we bound maximum and minimum slope to within a factor of 2 compared to the equilibrium profile.

4.3   2-D cellular model: avulsions and floodplains

The computational domain is discretized into square cells of length 500 m. There are three types of cells in our model: active channel (chan), abandoned channel (aban), and floodplain (fp). All cells have two elevations ("high" and "low") that we track throughout each run. All elevations are measured in meters.

Active channel

Active channel cells represent the current pathway of the river. There is one contiguous pathway for flow per time step. We selected a cell size such that modeled rivers are approximately one-fifth of the width of a cell; as a result, channel-scale processes (like meandering, crevasse splays, or other lateral-distance-dependent depositional effects) are not resolved.

The low elevation in each active channel cell represents the channel bed and is updated by transient diffusion as described in Eq. (3). Then, high elevations are set to the greater of (i) the high elevation at the last time step or (ii) one channel depth above the bed, such that

$$\left(\eta_{\text{chan,low}}\right)_t \text{ is given by Eq. (3)} \tag{4a}$$

$$\left(\eta_{\text{chan,high}}\right)_t = \max \begin{cases} \left(\eta_{\text{chan,high}}\right)_{t-1} \\ \left(\eta_{\text{chan,low}}\right)_t + h_{\text{chan}} \end{cases}, \tag{4b}$$

where t is the current time step and $t - 1$ is the prior one. This assumes that an aggrading river constructs levees that can contain its flow depth, but levees are not lowered if the river incises.

Other cell types become active channel cells whenever they are occupied by the active channel after an avulsion.

During this process, the low elevations of the new channel pathway are inset one channel depth down from the high elevations unless there is a channel that is already incised beyond this depth. This rule allows for channels to inherit levees (and superelevation) and does not further erode abandoned channel cells that are already incised more than one channel depth below their levees.

Abandoned channel

Abandoned channel cells include any cell that was once active but no longer contains water. These cells are still capable of attracting and repulsing pathfinding avulsions. Each cell has low and high elevations that reflect abandoned channel beds and levees, respectively. These elevations experience a linear healing rate that depends on healing mode but ultimately adjusts the channel-bed and levee elevations toward a specified endpoint (Sect. 4.3.2):

$$\eta_{\text{aban,low}} = \left(\eta_{\text{aban,low}}\right)_{t-1} + \left(A_{\text{fp,tot}} - \sigma\right) + H_{\text{low}} \quad (5a)$$

$$\eta_{\text{aban,high}} = \left(\eta_{\text{aban,high}}\right)_{t-1} + \left(A_{\text{fp,tot}} - \sigma\right) + H_{\text{high}}, \quad (5b)$$

where $A_{\text{fp,tot}}$ is the total overbank aggradation rate on the floodplain (meters per year; Sect. 4.3.2), and H_{low} and H_{high} are the healing rates (meters per year) applied to the low and high elevations, respectively.

Abandoned channel cells can become active channel cells if they are later occupied after an avulsion. Otherwise, they will become floodplain cells when

$$h_{\text{aban}} < \left(0.25 \cdot \overline{h}\right) \quad (6a)$$

$$h_{\text{aban}} = \left(\eta_{\text{aban,high}} - \eta_{\text{aban,low}}\right), \quad (6b)$$

where $\overline{h}$ is mean channel depth (meters) calculated over the entire length of the active channel at each time step. While healing gradually lowers h_{aban}, there is no process that can increase this relief other than revisitation by the active channel, in which case the cells will become active channel cells.

Floodplain

Floodplain cells are those never been visited by a channel or have completely healed after visitation. High and low elevations are equal for floodplain cells, except if they were once abandoned and have transitioned to floodplain (via the threshold in Eq. 6) they maintain their unequal elevations until healing is complete. Floodplain cells do not repulse or attract pathfinding avulsions. However, their remnant (and possibly unequal) elevations do affect setup and avulsion pathfinding via weighted random walk (Sect. 4.3.1).

Floodplain cells that retain any remnant relief are subjected to healing in the same manner as abandoned channel cells:

$$\eta_{\text{fp,low}} = \left(\eta_{\text{fp,low}}\right)_{t-1} + \left(A_{\text{fp,tot}} - \sigma\right) + H_{\text{low}} \quad (7a)$$

$$\eta_{\text{fp,high}} = \left(\eta_{\text{fp,high}}\right)_{t-1} + \left(A_{\text{fp,tot}} - \sigma\right) + H_{\text{high}}. \quad (7b)$$

4.3.1 Avulsion processes

Avulsion setup

Avulsions occur via three steps: (i) setup, (ii) initiation via triggering, and (iii) floodplain pathfinding. Avulsion setup (Slingerland and Smith, 2004) occurs from a combination of superelevation and flow-path gradient advantage. A cell is superelevated if the elevation of its channel bed is equal to or greater than at least one of its five neighboring cells (not including the three upstream cells; Fig. 3a and b) by some fraction of a mean channel depth:

$$\left(\eta_{\text{chan,low}} - \eta_{\text{adj,low}}\right) \geq (\beta - 1) \cdot \overline{h}. \quad (8)$$

We set $\beta = 1$, which requires the active channel bed to meet or exceed an adjacent cell's low elevation (Mohrig et al., 2000). As such, cells are considered superelevated when

$$\left(\eta_{\text{chan,low}} - \eta_{\text{adj,low}}\right) \geq 0. \quad (9)$$

Our results are insensitive to values of β between 0.5 and 1. In addition to superelevation, an avulsion in our model must have a local gradient advantage over its previous pathway. We calculate this gradient over the first step into surrounding cells, as opposed to over the entire pathway (cf. Ratliff et al., 2018).

Avulsion triggering

Once a portion of a river is superelevated, some triggering event is necessary to initiate an avulsion. Predicting natural triggers is challenging because they can take the form of floods, ice damming, bank erosion, woody debris dams, neotectonics, meander bend cutoffs, beaver dams, bar migration, or other events that allow flow to escape normal channel confinement (Harwood and Brown, 1993; Smith et al., 1998; Ethridge et al., 1999; Jones and Schumm, 1999; Mohrig et al., 2000; Slingerland and Smith, 2004; Gibling et al., 2010, Morón et al., 2017). With that said, we know that trigger recurrence can only be as long as observed avulsion periods in natural river systems, which range from 10^1 years on the Kosi River megafan to 10^3 years on the Mississippi Delta (Wells and Dorr, 1987; Aslan et al., 2005; Jerolmack and Mohrig, 2007).

We set an average avulsion trigger period of 30 years by specifying a fixed probability of a trigger occurring on any given time step. We select 30 years as it provides ample opportunity for a river to avulse, provided avulsion setup criteria are met. Since triggers cannot initiate avulsions in the absence of setup via superelevation (Slingerland and Smith, 2004), this effectively sets a lower limit on avulsion period, but the actual period may be longer if there are no superelevated river segments along the active channel when a trigger occurs.

Avulsion pathfinding

Whenever an avulsion trigger occurs, avulsion pathfinding initiates from a randomly selected active channel cell that meets the setup criteria. From here, the new channel path follows a steepness-weighted random walk if it remains in floodplain cells. Each step, the pathfinding avulsion can move into one of five cells (three downstream and two lateral). The cell is selected randomly, and the choices are weighted by steepness (see Table 1 for weighting scheme). Model outcomes are not sensitive over reasonable ranges of steepness weights, so long as all five directions are possible. The river is prevented from returning to its previous position and movement beyond the domain boundaries.

When a pathfinding avulsion is adjacent to an abandoned channel cell, the model checks to see if the abandoned channel cell is repulsive or attractive (Fig. 3c and d). Abandoned channel cells are repulsive when their levee heights above the adjacent floodplain (L_h; meters) are larger than some multiple of the pathfinding avulsion flow depth (h_{avul}; meters):

$$L_h > \alpha_R \cdot h_{avul} \tag{10a}$$
$$L_h = \left(\eta_{aban,high} - \eta_{appr,low} \right), \tag{10b}$$

where α_R is a non-dimensional repulsion factor, h_{avul} is the threshold channel depth calculated with diffusion theory (Paola et al., 1992) assuming the flow is channelized during pathfinding, and $\eta_{appr,low}$ is the low elevation in the adjacent cell from which the pathfinding avulsion channel approaches the abandoned channel. α_R is a threshold for how tall levees must be to repulse advancing flow. Lower values are more repulsive since the threshold to repel is lower. A value of zero means that any positive value of L_h would cause repulsion.

Abandoned channel cells are attractive when h_{aban} (meters) is larger than some fraction (α_A) of mean flow depth:

$$h_{aban} > \alpha_A \cdot \overline{h}. \tag{11}$$

α_A is a threshold value describing how much remnant relief an abandoned channel must retain to capture flow. Lower values are more attractive since it means only a small fraction of the original channel relief is required to be attractive. If captured, the pathfinding avulsion will move in the direction of the lowest $\eta_{aban,low}$. This will continue unless there are no abandoned channel cells into which flow can proceed, which can happen if the abandoned channel is discontinuous (Fig. 2), in which case the river is ejected back onto the floodplain and resumes steepness-weighted random walk.

Rivers that are repulsed or not captured by abandoned channels will proceed via steepness-weighted random walk until they exit the domain. If during pathfinding there are no viable moves, which can happen within floodplains bounded by abandoned channels that cannot be reoccupied (Fig. 2), the avulsion fails, all cells are reverted to their pre-avulsion states, and the model increments to the next time step. While this implementation of failed avulsion pathfinding is a simplification, it conceptually reflects healed crevasse splays

(Slingerland and Smith, 2004) and matches limited observational evidence, including among avulsions on the Rápulo River (Edmonds et al., 2022).

4.3.2 Floodplain processes

Floodplain processes are applied to all abandoned channel and floodplain cells. These processes include rules for (1) overbank deposition, (2) subsidence, and (3) abandoned channel healing.

Floodplain deposition and subsidence

We implement an overbank deposition rate that is constant along grid rows. As channels are considered small relative to the width of a cell, we assume that any distance-from-channel-dependent component to overbank sedimentation is contained within a single cell (cf. Bridge and Leeder, 1979; Pizzuto, 1987). Instead, and similar to Jerolmack and Paola (2007), the total floodplain aggradation for each row ($A_{fp,tot}$; meters per year) is the product of a base rate ($A_{fp,base}$; meters per year) and an additional term that increases linearly with the vertical distance between the highest elevation ($\eta_{high,max}$) in that row and the elevation of a far-field floodplain cell that has never been visited by the active channel ($\eta_{farfield}$). While simple, this depth-dependent scaling reflects a basic intuition that regions of the basin that are inundated to a greater depth beneath the highest levee (often the active channel) during flooding should receive more overbank sediment. The vertical distance term is non-dimensionalized by dividing by mean channel depth as averaged over the entire active channel. The base rate $A_{fp,base}$ increases downstream, described by a linear interpolation between an upstream and downstream boundary value, and reflects an increase in suspendible sediment (e.g., washload) downstream. Finally, we assume that total overbank deposition on the floodplain ($A_{fp,tot}$) cannot exceed subsidence (σ; meters per year):

$$A_{fp,tot} = \min \begin{cases} A_{fp,base} \cdot \frac{\eta_{high,max} - \eta_{farfield}}{\overline{h}} \\ \sigma \end{cases}. \tag{12}$$

Equation (12) deposits equal amounts of sediment on abandoned channel lows as highs and thus does not heal abandoned channels over time. Healing is handled separately and described in the following section. Finally, as a basic approximation of foreland basin style subsidence, we apply subsidence at each time step at constant rates. These rates vary spatially via linear interpolation between a pair of rates representing proximal and distal values, with the proximal rates being 2 times greater.
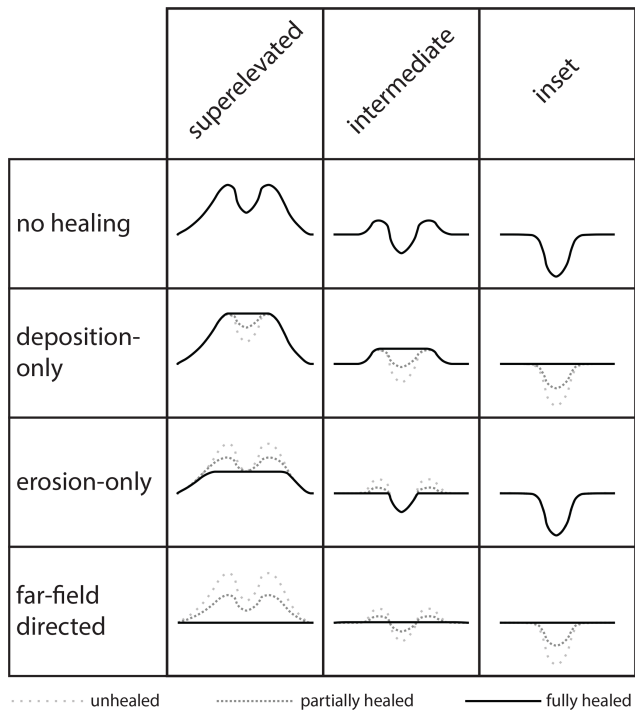
Figure 4. Potential healing modes for different initial conditions of abandoned channels. Each healing mode has different endpoints depending on the initial channel emplacement: deposition-only mode adjusts each abandoned channel cell's low elevation toward its high elevation, erosion-only mode adjusts high elevations toward low elevations, and far-field-directed mode adjusts both elevations towards the far-field floodplain elevation. As such, the deposition-only and erosion-only modes can result in topography that maintains positive topographic relief even once fully healed.

Abandoned channel healing

Despite the critical importance that floodplain topography and abandoned channel healing timescales play in affecting channel network evolution in avulsing systems (Jerolmack and Paola, 2007; Reitz et al., 2010), there is no consistent choice of rules for implementing this phenomenon in models of avulsion. In our model, we implemented different abandoned channel healing styles to explore how they influence avulsion dynamics and landscape evolution. Within these styles, abandoned channels can be healed "bottom up" as they are filled with sediment, "top down" as their levees are eroded, or have both elevations adjusted toward the far-field floodplain (Fig. 4).

All healing modes adjust high, low, or both elevations linearly until a given endpoint is reached (Fig. 4). The healing rates are set to

$$H_{\text{high}} = \alpha_{\text{H,high}} \frac{\overline{h}}{h_{\text{T}}} \tag{13a}$$

$$H_{\text{low}} = \alpha_{\text{H,low}} \frac{\overline{h}}{h_{\text{T}}}, \tag{13b}$$

where $\alpha_{\text{H,high}}$ and $\alpha_{\text{H,low}}$ are the healing rate parameters and have values that range from -1 to 1, and h_{T} is the characteristic time needed to heal one mean channel depth, which we set as 55 000 years. The value of h_{T} is necessarily speculative due to the lack of observational data on healing rates. We came to our value by first estimating the fastest reasonable timescale over which an $O : 10^0$ m deep abandoned channel (e.g., oxbow lake) can be filled when it is hydraulically connected to frequently flooding rivers (e.g., Cooper and Henry, 1989; Wren et al., 2008). This yields a minimum h_{T} of $O : 10^2$–10^3 yr. Abandoned channels must almost certainly heal slower than this rate, as most abandoned channels are distant from the active channel at any given time (Figs. 1 and 2), and net sediment deposition rates are known to decrease as observation window duration increases (Sadler, 1981; Schumer and Jerolmack, 2009). Next, we estimated an upper limit to h_T as the equilibration timescale of an abandoned channel via diffusion alone, which is on the order of $\frac{L^2}{\nu_{\text{fp}}}$ (Paola et al., 1992). For our case, L is a half-channel width (~ 50 m) and ν_{fp} can be approximated by hillslope diffusivity values (~ 0.005 m^2 yr^{-1}; Richardson et al., 2019). This yields a maximum h_{T} of $O : 10^5$ years. Finally, we chose a representative h_{T} between these two limits. Future work is needed to determine the validity of this assumed timescale, especially considering the importance of abandoned channels on affecting avulsion setup and pathfinding. Regardless, h_{T} is held constant between experimental runs, and we instead vary only the healing direction mode. The first healing mode (deposition only) raises abandoned channel lows toward levee tops, such that $\alpha_{\text{H,high}} = 0$ and $\alpha_{\text{H,low}} = 1$. The second healing mode (erosion only) lowers levees toward channel bases, such that $\alpha_{\text{H,high}} = -1$ and $\alpha_{\text{H,low}} = 0$. The third healing mode (far-field-directed) adjusts abandoned channel highs and lows toward the far-field floodplain elevation at rates of $\alpha_{\text{H,high}} = \pm 0.5$ TS2 and $\alpha_{\text{H,low}} = \pm 0.5$. TS3 In all cases, once topographic highs and lows have achieved their final healing endpoints (Fig. 4), $\alpha_{\text{H,high}}$ and $\alpha_{\text{H,low}}$ rates are set to 0.

4.4 Experimental design

We ran four series of model experiments to investigate how abandoned channel attraction, repulsion, and healing influence avulsion dynamics. A summary of non-experimental and experimental parameters is provided in Table 3.

The first series consists of a single base run with $\alpha_R = 4$, $\alpha_A = 0.25$, and far-field-directed healing. Setting $\alpha_R = 4$ means that flow is repulsed when levees are four times the height of the approaching flow; this allows some channels to be repulsive and others to not. Setting $\alpha_A = 0.25$ allows channels to capture flow so long as they are deeper than $1/4$ of a mean channel depth, consistent with flume experiments

Table 3. Model parameters used to generate figures.

Run duration (Myr)	Avulsion trigger period (years)	Healing timescale (h_T years)	Initialization length (meters)	Repulsion factor (α_R)	Attraction factor (α_A)	Healing mode	Figure no.
5	10	10 000	57 000	4.00	0.25	Far-field-directed	5
1	30	55 000	122 500	4.00	0.25	Far-field-directed	6, 8, 9
1	30	55 000	122 500	4.00	0.25	Far-field-directed, deposition-only, and erosion-only	7
5	30	55 000	122 500	−0.50 to 8.00	0.25	Far-field-directed	10
5	30	55 000	122 500	8.00	0.00 to 2.00	Far-field-directed	11
10	30	55 000	122 500	4.00	0.25	Far-field-directed, deposition-only, and erosion-only	12

(Reitz et al., 2010) that show old, filled-in abandoned channels acting as attractors with little remnant relief. For abandoned channel healing, we employed far-field-directed healing because its endpoint of a totally flat plane is equivalent to that of diffusion on a laterally infinite plane, approximating the effects of floodplain diffusion without the computational cost.

Our second set of runs explored the importance of abandoned channel repulsion on where, when, and why avulsions occur by varying α_R from −0.50 (most repulsive) to 8 (least repulsive), while holding $\alpha_A = 0.25$. Each run is a 5 Myr simulation using the far-field-directed healing mode. Next, a matching third set of runs was performed to investigate the effect of α_A by varying it from 2.00 (least attractive) to 0 (most attractive) and setting $\alpha_R = 8$. Our final set of runs investigated the role of abandoned channel healing mode without changing h_T (Fig. 4). We hold α_A and α_R constant between each 10 Myr run.

4.5 Analysis

We analyzed the planform appearance of generated topography and the location of avulsions for each run. For figures showing planform appearance (Figs. 5, 6 and 10–12), we show each cell's high elevation normalized relative to the η_{farfield} for its row. We did this because megafans are low-relief features, and the change in elevation along dip otherwise overwhelms the signal (Fig. 5). We quantified avulsion locations by recording the straight-line distance from the mountain front to each avulsion. These data were binned every 6.25 km and plotted as histograms showing the number of avulsions moving away from the upstream boundary. These values are normalized to the bin with the greatest occurrence. For Fig. 6, we measured and binned avulsion locations in the same way for a second run without relative

superelevation but normalized this histogram to that of the base run to display the overall reduced number of avulsions. We also analyzed avulsion locations by creating smoothed (50 kyr moving window average) curves of recorded distance to the mountain front that show how median and 95th percentile (i.e., distal) avulsion locations change over the course of simulations. Finally, we analyzed differences between the proximal and distal domains for our base run by tracking the along-strike position of the active channel at two distances (12.5, 50 km) from the mountain front for every time step (Fig. 7).

5 Model results

5.1 Base run and validation

We validated our model results by comparing model output for our base run with megafan topography from ICESat-2 (Neuenschwander et al., 2020) via the OpenAltimetry platform (Khalsa et al., 2020). ICESat-2 is a continuously measuring (10 kHz, ~ 0.7 m between points on the ground) satellite that collects vegetation-penetrating laser altimetry (Neuenschwander and Pitts, 2020). ICESat-2 offers greater precision than radar-derived elevation at the cost of limiting data collection to approximately north–south-oriented linear tracks. While our model does not aim to precisely simulate any specific fan, the simplified model recreates the essential features of mountain-front fluvial megafans. The 1-D elevation diffusion model reproduces rivers with appropriate channel depths and slopes, while the 2-D cellular model recreates the broad, low-relief, convex-up fan shape typical of megafans (Fig. 5). Along-dip comparisons on the Pucheveyem fan (Fig. 5) are also favorable, showing similar low-relief slopes ($\sim O : 10^{-3}$). These slopes change abruptly
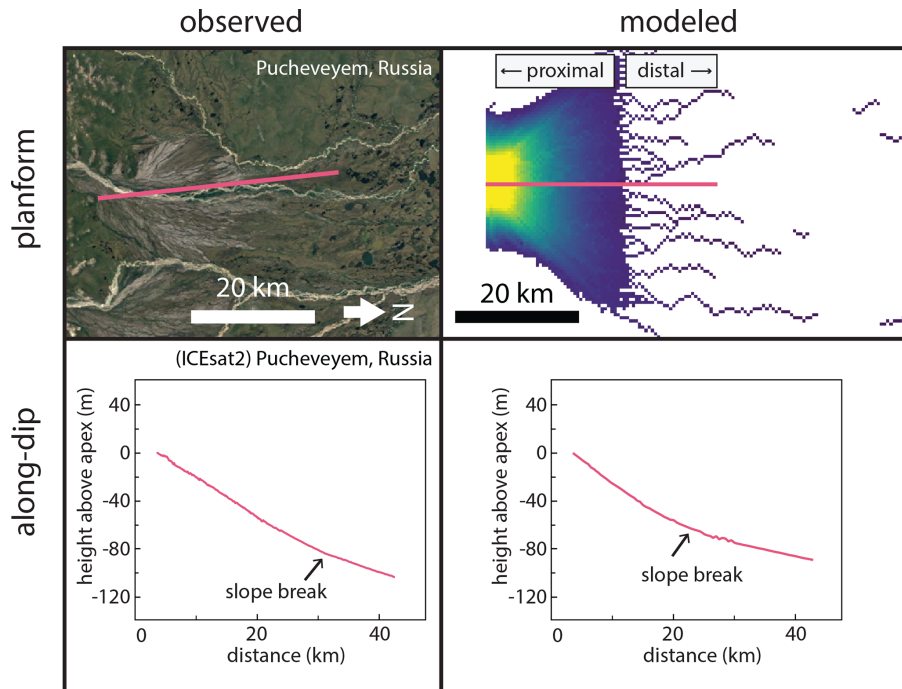
Figure 5. Megafan topography from model output compares favorably with real megafans, including delineation into distinct domains of slope. Color bar and explanation for modeled planform is provided in Fig. 6. Satellite images are USGS/NASA Landsat/Copernicus, © Google Earth.

at a topographic break marking the end of the fan topography, with a shallower gradient in the distal domain.

The model produces two distinct domains, herein called proximal and distal (Fig. 6a), despite no external parameters varying with distance to the mountain front, aside from a linearly decreasing subsidence rate and increasing overbank aggradation rate. Further, these two domains still emerge within the model even when these two parameters are held uniform. The two domains generated are consistent with earlier remote sensing observations (Fig. 1). The proximal domain is a zone of sediment distribution created by repeated avulsions; it has a steeper slope (Fig. 5) and the abandoned channels that create the topography are radially distributive (Fig. 6a). In this domain, frequent channel avulsion causes small lateral adjustments to river position (Fig. 7a), filling local topographic lows. Avulsion probability is highest at the apex because that is where sediment is introduced (Fig. 6b). In contrast, the distal domain is a zone with a dominantly tributive geometry; it has a shallower slope (Fig. 5) and is much more sparsely channelized (Fig. 6a). In this domain, the active channel switches between fewer, more persistent channels (Figs. 6a and 7a). Flow becomes confined to these more persistent channels because avulsions that occur upstream are quickly captured and routed into one of a finite number of pre-existing pathways (Fig. 7a). Distal abandoned channels that are occupied infrequently can partially or fully heal between revisitations, creating discontinuous alluvial

ridges (Figs. 2 and 6). Avulsion probability rapidly decreases past the fan boundary (Fig. 6b), and along-strike topographic relief is nearly flat, which compares favorably to previous observations of megafans (Hartley et al., 2010a; Bernal et al., 2011). Notably, we reproduce these channel and megafan features despite the absence of bounding rivers or other external topographic controls that are seen on some modern megafans (Fig. 1e and f).

5.2 How abandoned channels affect avulsion dynamics

Abandoned channels affect the timing and location of avulsions in four different ways: (1) superelevation shortcutting, (2) inheritance, (3) post-avulsion diffusion of the channel-bed, and (4) confluence aggradation. Each is discussed below.

We implemented avulsion setup by measuring superelevation of an active channel relative to surrounding floodplain topography (Eq. 2; Fig. 3). To investigate the effect of abandoned channels on this setup, we performed an additional run that is equivalent to our base run in Fig. 6 except for requiring each cell to aggrade a specified fraction ($\beta = 1$) of a channel depth between each avulsion (Eq. 1; Fig. 6b). Compared to this run, the base run had a greater number of avulsions, especially on the megafan surface downstream of the apex (Fig. 6b). Further, the run using Eq. (2) had a mean time between avulsions of 32 years, compared to 57 years for the run using Eq. (1). Measuring superelevation relative to flood-
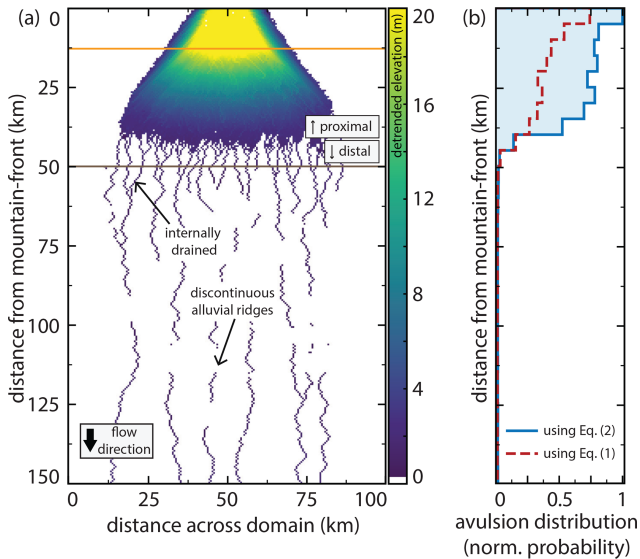
Figure 6. (a) Planform output of detrended high elevations from the base run. The color bar is chosen such that negative or near-zero detrended values appear white. The location of the active channel is not shown. The model produces two distinct domains (proximal and distal) in addition to several marked features which compare well with observed megafans (Fig. 1). Horizontal orange and dark brown lines show the proximal and distal measurement locations, respectively, for Fig. 7a. **(b)** A histogram (bin width of 6.25 km) showing the downstream distribution of avulsion loci. Blue line corresponds to the model run shown in panel **(a)**, whereas the dashed red line is an equivalent run that differs by requiring one full channel depth of aggradation to achieve superelevation (Eq. 1) instead of measuring elevation relative to adjacent cells (Eq. 2). The run using Eq. (2) had a mean time between avulsions of 32 years, compared to 57 years for the run using Eq. (1). Vertical axis scale for panel **(b)** is the same as that for panel **(a)**.

plains allows local topographic lows associated with former abandoned channels to provide attractive locations for avulsion initiation, shortcutting superelevation timescales (Jerolmack and Mohrig, 2007). Therefore, a densely channelized proximal domain generates additional superelevation opportunities, spatially concentrating avulsions (Fig. 6b).

Abandoned channels also affect avulsion setup indirectly through reoccupation mechanics. Superelevation is inherited when avulsive flows reoccupy former abandoned channels. In a superelevated channel reach, an avulsion will strand superelevated portions of the river that are downstream of the avulsion locus (discontinuous alluvial ridges in Fig. 6a). In this way, avulsions can leave behind abandoned channels that may require minimal aggradation to achieve superelevation if they are reoccupied before being healed, particularly if those channels are themselves adjacent to abandoned channel topography that provides relative superelevation.

In our model, avulsion setup is also affected by local effects immediately after avulsions due to transient diffusion. This occurs in two ways. Firstly, superelevated cells up-
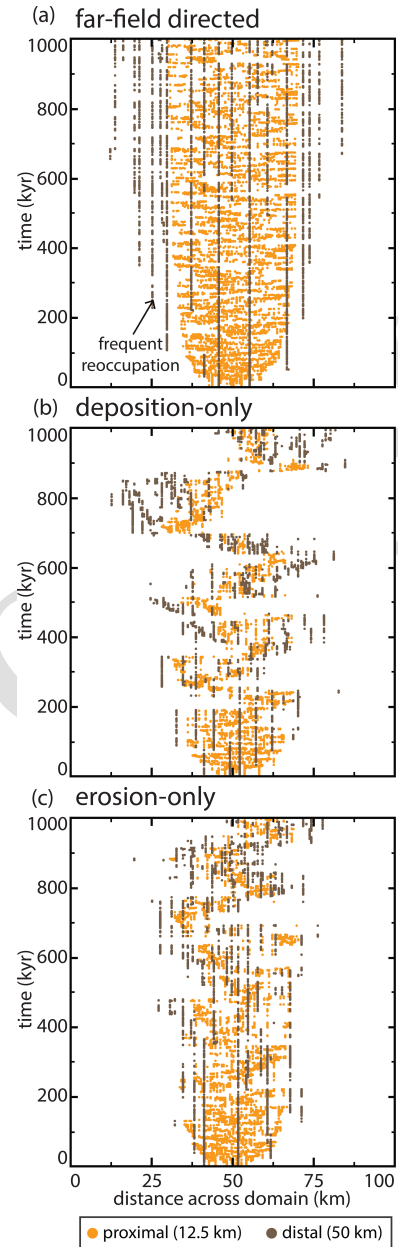
Figure 7. Active channel position histories over 1 Myr at two distances from the mountain front for three runs. Distances to the mountain front are illustrated via horizontal bars in Figs. 6a and Fig. 12a. In each run, only one channel position is possible per time step. **(a)** A run using the same parameters as Fig. 6. Note frequent and continued reoccupation for distal river positions. Panels **(b)** and **(c)** show runs identical to those in panel **(a)**, except the healing modes are deposition-only and erosion-only, respectively (Fig. 12a). These runs show similar behavior to that in panel **(a)** in early years but transition to lobe-switching behavior.
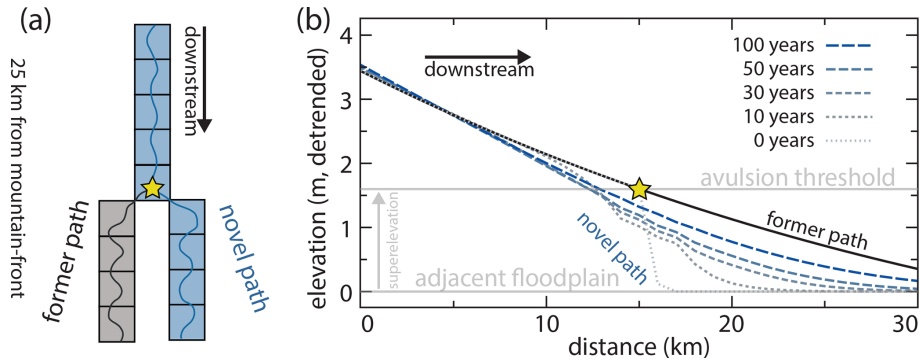
Figure 8. Model example showing channel evolution immediately after an avulsion at a node marked by a star. **(a)** Planform arrangement of the parent channel and avulsion node, with both pathways of equal length. **(b)** Detrended elevation of the parent channel (relative to the adjacent floodplain) and new avulsion pathway upstream and downstream of the avulsion node. Immediately prior to the avulsion (black line), all cells upstream of the avulsion node are superelevated and are equally likely to avulse if a trigger occurs. After the avulsion, gradual knickpoint propagation upstream reduces superelevation. Downstream of the avulsion site, there is significant deposition that reduces the time to superelevation.

stream of the avulsion locus are not instantly lowered but instead require time for the knickpoint to propagate upstream (Fig. 8). In our simulation, the post-avulsion upstream reduction in channel-bed superelevation proceeded gradually, migrating only several kilometers 100 years after an avulsion (Fig. 8). In this way, an avulsion does not instantly undo the avulsion setup of cells upstream and future triggers can still cause avulsions to occur over this domain. Secondly, immediately downstream of an avulsion locus there is significant aggradation; a channel can diffuse nearly a meter of sediment into a downstream active channel cell within a decade (Fig. 8). In the case that these downstream cells are themselves already nearly superelevated, this can provide sufficient aggradation above the adjacent floodplain to set up these cells. This effect is even more pronounced when new active channel cells are adjacent to abandoned channel lows and thus have lower superelevation thresholds.

In our model, we observed abandoned channel confluences wherever a pathfinding flow is captured by a previous abandoned channel. Captured channels follow steepest-descent pathfinding within the network of occupiable abandoned channel cells. Within the distal, tributive domain, the number of possible abandoned channel pathways that can be occupied decreases with increasing distance from the mountain front (Figs. 6a and 7a). This allows locations downstream of confluences to be more continuously occupied while the flow switches pathways upstream. This has important effects on avulsion because more aggradation occurs downstream of the tributary junction. Consider a scenario where avulsions on the fan always route flow into one of two possible paths (Fig. 9). The pathway downstream of the confluence is occupied 100 % of the time while each parent pathway is occupied approximately half of the time. As channel-bed aggradation occurs only during active channel occupation, aggradation downstream of the confluence can therefore be greater

than that observed in either upstream pathway (Fig. 9c). As such, in the distal domain, abandoned channel reoccupation should preferentially focus avulsions downstream of abandoned channel confluences.

5.3 Abandoned channel repulsion

We observed the effects of varying α_R on both planform appearance and the location of avulsions with a constant α_A (Fig. 10). Increasing repulsion (decreasing α_R) extends the proximal domain farther downstream; increasingly repulsive runs are increasingly distributive and generate fewer tributary confluences (Fig. 10a). Further, runs that are highly repulsive do not generate the abrupt downstream change in avulsion frequency seen when $\alpha_R \geq 1.00$. Instead, highly repulsive runs show relative avulsion frequencies that follow a power-law-like distribution with distance from the mountain front (Fig. 10a).

The proximal domain propagates farther downstream when α_R is smaller (more repulsive) because avulsion location propagates farther downstream (Fig. 10b). While all avulsion location curves show a downstream progradation of avulsion locations during runs as the fan grows, both the median and 95th percentile shift downstream between runs with decreasing α_R when $\alpha_R \leq 1.00$ (i.e., where avulsive flows must be equal to or greater than levee heights above surrounding floodplains to reoccupy). Median avulsion locations are less affected than 95th percentile curves, indicating that distribution skewness increases.

Increasing repulsion (decreasing α_R) pushes avulsions farther from the mountain front because flow in the proximal domain is concentrated into fewer channels, allowing for sediment (and therefore superelevation) to propagate farther downstream (Fig. 10). As a contributing effect, runs with lower α_R create more internally drained basins that them-
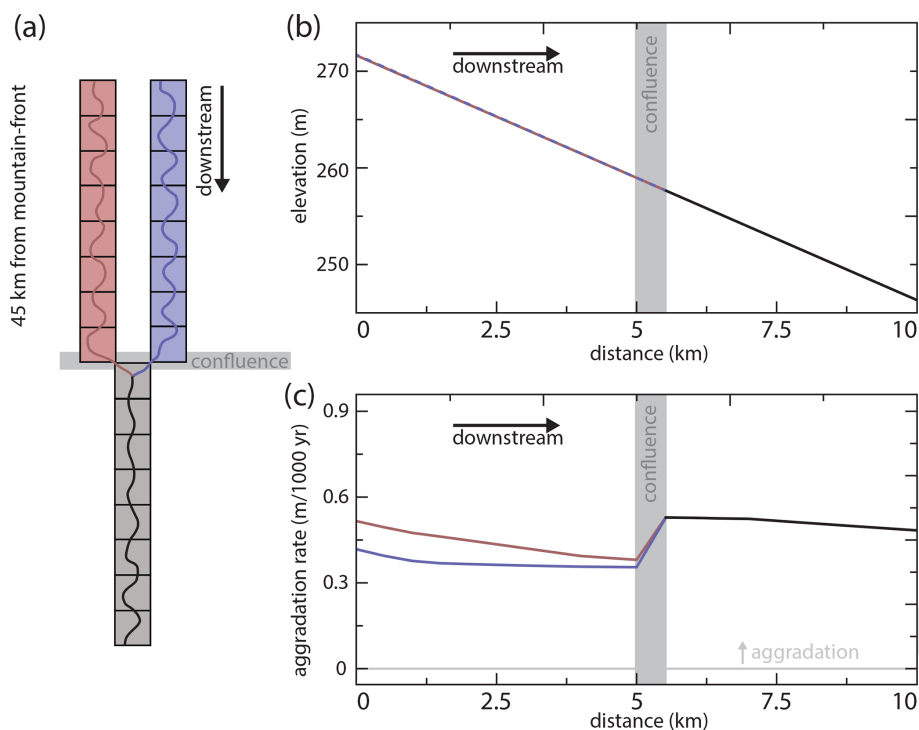
Figure 9. Model experiment showing channel evolution at an abandoned channel confluence. **(a)** Planform arrangement where the channel avulses between the red and blue pathways whenever normal avulsion criteria are satisfied. **(b)** Elevations of the red, blue, and gray channel segments upstream and downstream of the confluence. These elevations are not detrended. The blue channel profile is dashed to not obscure the red channel profile. **(c)** Aggradation rates over a 3000-year period along the three channel segments. Repeated avulsions mean that the red and blue channels alternate deposition, while the gray channel downstream is constantly occupied leading to a faster aggradation downstream of the confluence.

selves cause avulsions to fail. Since failed avulsions cause the time step to increment without changing river positions, the time between successful avulsions is greater in runs with many failed avulsions, and sediment can thus propagate farther along active channels. This encourages channels in the distal part of the model to superelevate and avulse more often.

5.4   Abandoned channel attraction

Abandoned channel attraction dynamics also impact both avulsion locations and planform appearance during model runs (Fig. 11). With a constant α_R and increasing abandoned channel attraction (decreasing α_A), the transition from distributive to tributive domains shifts up-domain and fan width increases (Fig. 11a). When α_A is large (low attractiveness), model output resembles a series of weighted random walks because abandoned channels rarely capture flow and steepness weighted random walk determines channel position. Like the repulsion simulations, both the median and 95th percentile avulsion locations are affected by changing attraction parameters (Fig. 11b). Decreasing α_A (increasing attractiveness) pulls avulsions towards the mountain front, and the greatest change is for α_A between ~ 0.50 and 1.50. Mini-

mal change occurs for α_A values above and below this range. In contrast, when α_A increases (attractiveness decreases), the fan lengthens and avulsions occur farther down domain because fan surfaces host abundant abandoned channels that influence avulsion dynamics. This interpretation is supported by the avulsion histograms, where low-attractiveness runs show a non-zero avulsion frequency plateau in the distal reaches and a more gradual downstream reduction in frequency than in more attractive runs (Fig. 11a).

5.5   Healing mode

The healing mode determines how abandoned channels are gradually removed from the floodplain. By conducting 10 Myr base runs with different healing modes, we found that the deposition-only and erosion-only runs generated fans that nearly entirely filled up the simulation space over the course of several million years (Fig. 12). This occurs because the remnant topography of abandoned channels was never entirely removed by healing between visitations (Fig. 4). This is true even for the erosion-only run as, by definition, channels that achieve superelevation before abandonment have bases that are higher than surrounding floodplains. Since healing in erosion-only runs terminates once levees reach channel beds,
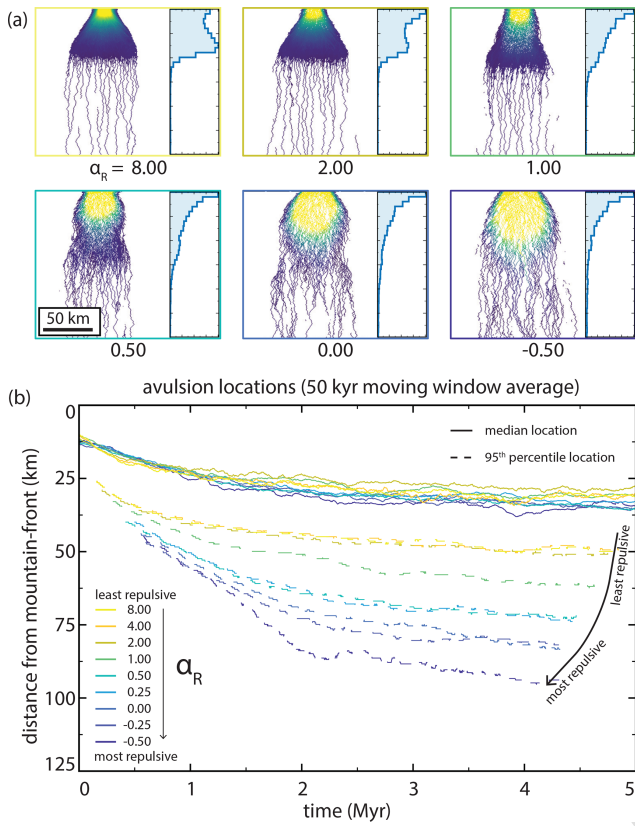
Figure 10. The effect of abandoned channel repulsion on **(a)** planform appearances and normalized avulsion location histograms and **(b)** median avulsion locations through time. Decreasing α_R causes avulsion location to move downstream. These changes are more pronounced for 95th percentile locations. Color scale for inset planform appearances is the same as in Fig. 6.

superelevated abandoned channel beds on the floodplain remain indefinitely.

Healing mode affects avulsion location and introduces a new dynamic for fan growth. In erosion-only runs, the avulsion location propagates the farthest into the basin (Fig. 12b). Interestingly, the median and 95th percentile time series for deposition-only and erosion-only avulsion locations show spikes that represent avulsion location rapidly moving toward the mountain front. These spikes represent lobe switching events, where avulsion loci shifted proximally as depositional space lower on the fan is filled and apical avulsions reroute flow to new regions on the fan surface (Fig. 7b and c; supplemental videos 1–3; https://doi.org/10.5446/54887). This compares well to observations of real-world megafans where deposition is interpreted to have occurred on discrete lobes (Chakraborty et al., 2010; Zani et al., 2012; Assine et al., 2014; Weissmann et al., 2015; Pupim et al., 2017). Lobe switching emerges in the model when deposition is localized in a particular region sufficiently long for a lobate area to become raised relative to other areas on the floodplain. This lowers the effective slope of this pathway, leading to a slope
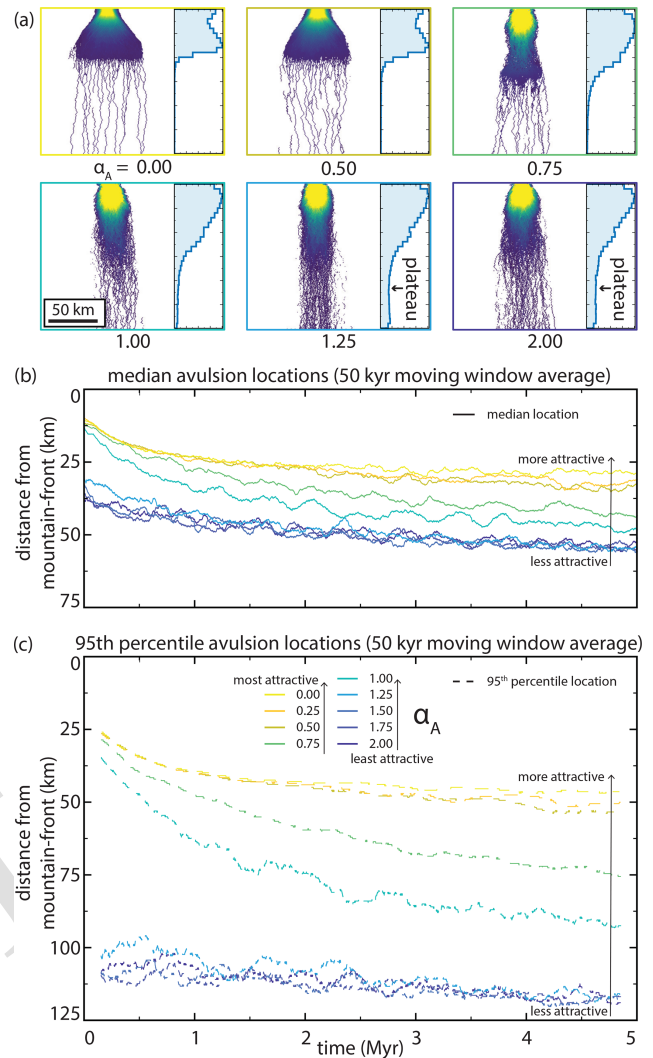
Figure 11. The effect of abandoned channel attraction on **(a)** planform appearances and normalized avulsion location histograms, and **(b, c)** characteristic avulsion locations through time. α_A legend and x-axis scale in panel **(c)** applies to **(b)** as well. Note the difference in y-axis range between panels **(b)** and **(c)**. Between α_A values of 0.50 and 1.50, increasing α_A causes predictable increases in the distance between the mountain front and median and 95th percentile avulsion locations. These changes are more pronounced for 95th percentile locations, indicating greater skewness. Color scale for inset planform appearances is the same as in Fig. 6.

disadvantage over other regions on the floodplain. Future apical avulsions can then redirect flow to these other lower regions due to slope-weighted pathfinding, leading these lower regions to themselves eventually become raised and begin the cycle anew. Lobe switching does not occur during the earliest stages of fan growth because slopes are relatively steep on all faces of the fan, and there is thus little intervening topography that could prevent an avulsing river from accessing other areas on the fan surface.
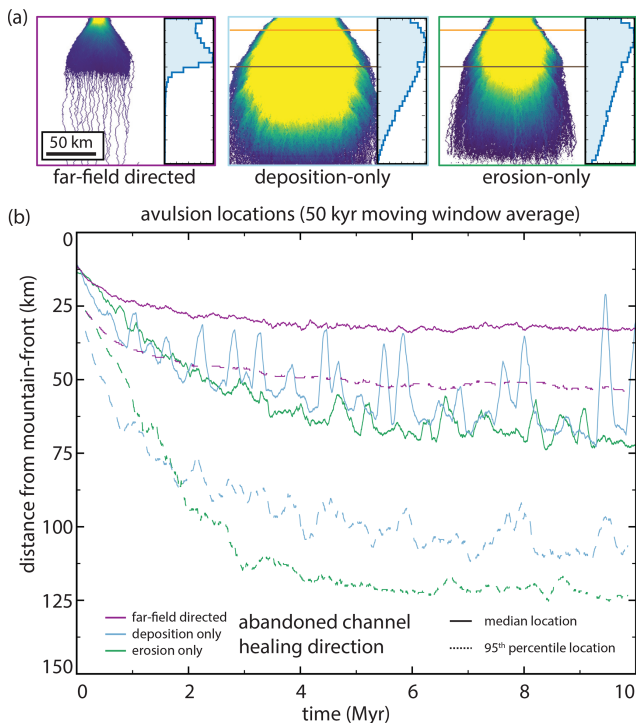
Figure 12. The effect of healing mode on **(a)** planform appearances and normalized avulsion location histograms and **(b)** characteristic avulsion locations through time. Runs are identical other than employing different abandoned channel healing modes. Horizontal orange and dark brown lines show proximal and distal (respectively) distances from mountain fronts for Fig. 7b (deposition only) and Fig. 7c (erosion only). Color scale for inset planform appearances is the same as in Fig. 6.

In contrast to the deposition-only and erosion-only runs, the far-field-directed simulation achieved dynamic equilibrium relatively quickly and maintained a well-defined boundary between the proximal and distal domains for the remainder of the run. This occurs because it is the only healing mode that completely removes abandoned channel topography from floodplains. As such, this is the only healing mode that erases the topographic, attractive, and repulsive "memories" (*sensu* Reitz et al., 2010) of abandoned channels. Lobe switching on the same timescale is not observed in these runs because, unlike the deposition-only and erosion-only runs, far-field-directed runs do not preserve topography indefinitely and alluvium is removed too quickly to build up regional slopes that can effectively resist pathfinding (Fig. 7). Thus, while lobe switching seems to have somewhat different frequencies based on whether abandoned channel healing is dominated by infilling or levee erosion, the overall existence of lobe switching on this $O : 10^5$ timescale is sensitive to the preservation potential of superelevated channel beds and alluvial ridges.

It is important to note that both the erosion-only and deposition-only runs exhibited the typical separation of planform space into two domains as they prograded, until the proximal domain encountered the edge of simulation space and the only further adjustment that could occur was via vertical aggradation. Despite this, the deposition-only and erosion-only runs appear to have less abrupt downstream avulsion frequency changes compared to the far-field-directed one because the histograms are time integrated and reflect avulsion locations throughout the entire history of the run, including during progradation (Fig. 12a).

6 Discussion

6.1 Model sensitivity to non-experimental parameters

Our model is generally insensitive to small variations within reasonable ranges for most parameters presented in Tables 1 and 2, including values for random walk weights, minimum superelevations (β), overbank aggradation base rates $A_{\mathrm{fp,base}}$, subsidence rates (σ), initialization lengths, abandoned channel healing timescales (h_{T}), and incoming specific discharge and sediment supplies. One exception is that the overbank aggradation rate and subsidence rate at the bottom boundary of the domain must be equal to satisfy the downstream boundary condition, and if subsidence is much larger than aggradation upstream, the basin can sag due to underfilling over stratigraphic timescales. We performed test runs with more functional changes, including runs that employed uniform subsidence (as opposed to foreland basin style subsidence), overbank deposition base values ($A_{\mathrm{fp,base}}$) that did not change with distance to the mountain front, or channel depths (h) and avulsion flow depths (h_{avul}) that did not vary along channel. In all cases, we still recreated the fundamental findings of two distinct emergent domains and the effects of abandoned channel repulsion, attraction, and healing on avulsion location.

6.2 Abandoned channels in avulsion models

Our model was designed to investigate the role of abandoned channels as both topographic repulsors and attractors during avulsion pathfinding. In doing so, we demonstrated effects on avulsion location and planform landscape evolution. We showed that abandoned channels affect the frequency and position of avulsions. Importantly, we demonstrated that the typical low-relief megafan with a transition from proximal (distributive, densely channelized) to distal (tributive, sparsely channelized) domains originates only when avulsion repulsion is infrequent and attraction is frequent (Figs. 10 and 11). As such, when creating avulsion models, it is worth explicitly addressing abandoned channel creation, rate of healing, mode of healing, and interactions with future avulsion setup and pathfinding because these factors fundamentally change the avulsion dynamics and planform appearance of fluvial systems.

Previous stratigraphic models that simulate accumulation of channel bodies in a 2-D strike-oriented cross section have had to employ rules in order to emplace successive channels without resolving planform pathfinding (Sect. 2). These rules typically are random, compensation (lowest elevation), or clustered (channel emplacement occurs near previous channel location). These rules create important differences in simulated alluvial stratigraphy (Chamberlin and Hajek, 2015); however, the floodplain conditions that lead to each rule are unknown. Our results show that the position of successive channels after avulsion follows different emplacement rules in proximal and distal domains for moderate attraction and repulsion (Fig. 7). In the proximal domain, avulsion pathways follow steepest descent that should generate compensational stratigraphy by seeking local, not global, topographic lows (Fig. 7). This compares well to limited observational data showing that most avulsions initiate into topographic lows and travel relatively small lateral distances before joining abandoned channels (Edmonds et al., 2016; Valenza et al., 2020). In our deposition-only and erosion-only runs, emergent lobe switching provides an additional process that can control channel positions, creating both clustering (channel switching within lobes) and compensation (lobes switch to compensate; Figs. 7 and 12). In the distal domain, channels are nearly perfectly clustered because flow routing switches between a small number of active channels in a network, each of which can heal if they are not revisited for a sufficient amount of time (Fig. 7). This compares better to the experimental model and flume observations of Jerolmack and Paola (2007) and Reitz et al. (2010). As a caveat, when abandoned channels influence pathfinding, our model shows that it is not always possible for avulsions to find the globally lowest point in the whole domain for a given cross section (cf. Bridge and Leeder, 1979) because there may be high topography in between that prevents pathfinding. This is particularly evident in the lobe switching shown in Fig. 7b and c, where the global lowest point may exist outside of lobe deposition, but no viable route exists to reach that point.

6.3 Floodplain topography and evolution

Our model shows that lobe switching on megafans only appears under certain abandoned channel healing rules (Figs. 7 and 12). Floodplain topography, including abandoned channels, is thus a critical control on avulsion dynamics and landscape evolution and modelers who wish to recreate foreland basin topography must be conscious of how they choose to implement abandoned channel healing. While our results indicate that the preservation of abandoned channel topography between avulsions is necessary for lobe switching to emerge, further research can be directed towards uncovering other necessary conditions, and thus whether it is appropriate to assume that the presence of lobe switching on real-world fans is a predictor of abandoned channel healing mode. Regardless, the dependence of lobe switching on abandoned

channel healing mode within our model emphasizes Jerolmack and Paola's (2007) identification of the remarkable lack of knowledge regarding the competing processes of topographic construction and destruction on floodplains. The principal topographic features of floodplains in aggradational (*sensu* Weissmann et al., 2015) settings appears to be abandoned channels, including both topographic highs and lows (Fig. 2). Understanding the extent to which abandoned channels and floodplain topography control avulsion dynamics in natural systems requires a better understanding of floodplain topography.

Given the extent of these unknowns, considerable insight about floodplain evolution could be gained from highly detailed investigations of channel levees and beds before and after avulsions. Such investigations have been employed for abandoned channels in deltaic settings (e.g., Carlson et al., 2020), and similar work could reveal the channel-scale mechanics of abandoned channel attraction and repulsion in natural fluvial settings. Longitudinal studies of this nature could also understand the rate at which abandoned channels are healed (and thus no longer affect pathfinding) and the direction or mode in which they are healed, which we found to have important implications on avulsion dynamics (including lobe switching) and long-term planform morphology (Fig. 12). If abandoned channel healing rates are observed to vary spatially (for instance with distance along strike from the active channel or distance along dip from the mountain front), this could motivate further modeling efforts. It may be that healing proceeds in different directions and at different rates in different settings in the basin, which will have important impacts on the spatial variation of avulsion dynamics and planform morphologies. We note that detailed work on the time fate of topographic highs associated with abandoned channels is especially lacking in the body of literature. Finally, observations of avulsions in progress would help with understanding the appropriateness of our parameters α_R and α_A.

6.4 Next steps and predictions for comparison with field sites

We make several predictions that can motivate future observational and field studies. To begin, one key prediction is that in the proximal portions of foreland basins, avulsions should be most frequent on the surfaces of megafans (e.g., Fig. 6b). These results compare favorably to the limited data available (Valenza et al., 2020) and can be tested by future observations of avulsions in the remote sensing record. The emergence of future datasets on real-world avulsions should be able to confirm or deny the predicted abrupt change in relative avulsion frequency with increasing distance from mountain fronts on megafans (Fig. 6b). Avulsion location data should also allow testing of other predictions from our model, including that avulsion in the distal domain of aggradational settings is more common immediately downstream

of abandoned channel confluences due to a greater total occupancy duration and therefore greater total aggradation than either parent pathway immediately upstream (Fig. 8). Finally, our model suggests that stratigraphic systems with evidence for clustering of channel avulsions (e.g., the Ferris Formation; Hajek et al., 2010) may have greater degrees of abandoned channel influence via attraction or lobe switching than systems that appear more randomly distributed (e.g., the Williams Fork Formation; Chamberlin et al., 2016).

7 Conclusion

Abandoned channels are pervasive on megafans in modern foreland basin settings. Megafans also have some of the highest avulsion rates in the observational record, which necessitates considering the role of abandoned channels on avulsion dynamics and planform evolution in modeling efforts. We developed and presented a model that tests the interaction between abandoned channels and an avulsing river. Our model intrinsically generates two distinct domains, proximal and distal, in good comparison with remote sensing and previous research. We demonstrated that abandoned channels may shortcut avulsion superelevation timescales in these settings by providing topographic lows adjacent to potential avulsion loci, by providing remnant superelevation that can be inherited by future captured avulsions, including downstream of abandoned channel confluences, and by transient knickpoint propagation that allows superelevated rivers to remain superelevated upstream of the initial avulsion. The upshot of these factors is that avulsions are proportionately much more common over the proximal distributive domain compared to the distal tributive one. We showed that tuning the degree to which abandoned channel repulsion and attraction occur in simulations causes predictable changes in avulsion location during those runs, whereby increasing repulsion pushes avulsions farther from the mountain front, and increasing attraction pulls them closer. Next, we demonstrated the important role that abandoned channel healing mode has on gross planform morphology, particularly over deep time, and that the proximal domain should grow until filling all available space in systems that heal via only deposition or only erosion. Finally, we have highlighted opportunities for future work by field workers and remote sensors in understanding the role that floodplain topography plays on avulsion dynamics and the fate of floodplain abandoned channel topography.

Appendix A

Table A1. Notation.

Symbol	Name	Units
A	non-dimensional constant	non-dimensional
A_{chan}	in-channel aggradation rate at some location	meters per year
$A_{\text{fp,base}}$	base rate component of overbank aggradation	meters per year
$A_{\text{fp,tot}}$	total overbank aggradation rate on the floodplain	meters per year
α_{A}	attraction factor	non-dimensional
$\alpha_{\text{H,high}}$	healing rate parameter for high elevations	non-dimensional
$\alpha_{\text{H,low}}$	healing rate parameter for low elevations	non-dimensional
α_{R}	repulsion factor	non-dimensional
β	channel depth fraction	non-dimensional
c_{f}	drag coefficient	non-dimensional
C_0	bed sediment concentration	non-dimensional
$\eta_{\text{aban,high}}$	abandoned channel-levee elevation	meters
$\eta_{\text{aban,low}}$	abandoned channel-bed elevation	meters
$\eta_{\text{adj,low}}$	channel-bed elevation for a cell adjacent to the active channel	meters
$\eta_{\text{appr,low}}$	low elevation in the cell from which a pathfinding avulsion approaches an abandoned channel	meters
$\eta_{\text{chan,high}}$	levee elevation for an active channel cell	meters
$\eta_{\text{chan,low}}$	channel-bed elevation for an active channel cell	meters
η_{farfield}	elevation of a far-field floodplain cell that has never been visited by the active channel	meters
$\eta_{\text{fp,high}}$	floodplain elevation, high	meters
$\eta_{\text{fp,low}}$	floodplain elevation, low	meters
$\eta_{\text{high,max}}$	the highest active, abandoned, or floodplain high elevation in a given row	meters
h_{aban}	remnant depth of an abandoned channel	meters
h_{avul}	flow depth of the pathfinding avulsion	meters
h_{chan}	active channel depth	meters
h_{T}	characteristic time needed to heal one mean channel depth	years
$\overline{h}$	mean flow depth	meters
H_{low}	healing rate for low elevations	meters per year
H_{high}	healing rate for high elevations	meters per year
L_{h}	levee height above approaching floodplain	meters per year
q	normalized water discharge per unit basin width	square meters per year
ρ_{sediment}	density of sediment	kilograms per cubic meter
ρ_{water}	density of water	kilograms per cubic meter
S	sediment specific gravity	non-dimensional
σ	subsidence rate	meters per year
t	time	years
T_{A}	time needed to achieve superelevation	years
ν	diffusivity	square meters per year
x	space	meters

Code availability. Our model code is written in MATLAB and is publicly and freely available (under the GPL v3 license) via GitHub at the following DOI link: https://doi.org/10.5281/zenodo.5576789 (Martin and Edmonds, 2021).

Data availability. Research data (model outputs) are available via Zenodo under the Creative Commons Attribution 4.0 International license. Data can be accessed at the following DOI link: https://doi.org/10.5281/zenodo.6574084 (Martin and Edmonds, 2022d).

Video supplement. A video supplement (supplemental videos 1–3) is uploaded to the AV portal of TIB Hannover under the CC BY-NC-SA 3.0 DE license. The videos can be accessed at the following DOI links:

- https://doi.org/10.5446/54887 (Martin and Edmonds, 2022a) – Martin and Edmonds avulsion model supplemental video 1;

- https://doi.org/10.5446/54888 (Martin and Edmonds, 2022b) – Martin and Edmonds avulsion model supplemental video 2;

- https://doi.org/10.5446/54889 (Martin and Edmonds, 2022c) – Martin and Edmonds avulsion model supplemental video 3.

.

Author contributions. HKM and DAE conceptualized and designed the research and developed the code. HKM collected and analyzed the data, wrote the manuscript, and prepared the figures. DAE supervised the research and reviewed and edited the manuscript.

Competing interests. The contact author has declared that neither they nor their co-author has any competing interests.

Disclaimer. Publisher's note: Copernicus Publications remains neutral with regard to jurisdictional claims in published maps and institutional affiliations.

Acknowledgements. We would like to thank Ben Peters for assistance with preparation of Fig. 1. We would also like to thank Gary Weissmann and Jeffery Valenza for helpful conversations about rivers in foreland basins. Finally, we would like to thank Ellen Chamberlin, Eric Barefoot, and one anonymous reviewer for helpful suggestions that improved the manuscript.

Financial support. Harrison K. Martin was supported by NASA FINESST grant no. 80NSSC21K1598. Harrison K. Martin and Douglas A. Edmonds were supported by US National Science Foundation grant no. EAR-1911321.

Review statement. This paper was edited by Paola Passalacqua and reviewed by Ellen Chamberlin, Eric Barefoot, and one anonymous referee.

References

Allen, J. R. L.: Studies in fluviatile sedimentation: an exploratory quantitative model for the architecture of avulsion-controlled alluvial suites, Sediment. Geol., 21, 129–147, https://doi.org/10.1016/0037-0738(78)90002-7, 1978.

Aslan, A., Autin, W. J., and Blum, M. D.: Causes of River Avulsion: Insights from the Late Holocene Avulsion History of the Mississippi River, U.S.A., J. Sediment. Res., 75, 650–664, https://doi.org/10.2110/jsr.2005.053, 2005.

Assine, M. L.: River avulsions on the Taquari megafan, Pantanal wetland, Brazil, Geomorphology, 70, 357–371, https://doi.org/10.1016/j.geomorph.2005.02.013, 2005.

Assine, M. L. and Soares, P. C.: Quaternary of the Pantanal, west-central Brazil, Quatern. Int., 114, 23–34, https://doi.org/10.1016/S1040-6182(03)00039-9, 2004.

Assine, M. L., Corradini, F. A., do Pupim, F. N., and McGlue, M. M.: Channel arrangements and depositional styles in the São Lourenço fluvial megafan, Brazilian Pantanal wetland, Sediment. Geol., 301, 172–184, https://doi.org/10.1016/j.sedgeo.2013.11.007, 2014.

Bernal, C., Christophoul, F., Darrozes, J., Soula, J.-C., Baby, P., and Burgos, J.: Late Glacial and Holocene avulsions of the Rio Pastaza Megafan (Ecuador–Peru): frequency and controlling factors, Int. J. Earth Sci. (Geol. Rundsch.), 100, 1759–1782, https://doi.org/10.1007/s00531-010-0555-9, 2011.

Bokulich, A.: Explanatory Models Versus Predictive Models: Reduced Complexity Modeling in Geomorphology, in: EPSA11 Perspectives and Foundational Problems in Philosophy of Science, Springer, Cham, 115–128, https://doi.org/10.1007/978-3-319-01306-0_10, 2013.

Bridge, J. S. and Leeder, M. R.: A simulation model of alluvial stratigraphy, Sedimentology, 26, 617–644, https://doi.org/10.1111/j.1365-3091.1979.tb00935.x, 1979.

Bryant, M., Falk, P., and Paola, C.: Experimental study of avulsion frequency and rate of deposition, Geology, 23, 365–368, https://doi.org/10.1130/0091-7613(1995)023<0365:ESOAFA>2.3.CO;2, 1995.

Buehler, H. A., Weissmann, G. S., Scuderi, L. A., and Hartley, A. J.: Spatial and Temporal Evolution of an Avulsion on the Taquari River Distributive Fluvial System from Satellite Image Analysis, J. Sediment. Res., 81, 630–640, https://doi.org/10.2110/jsr.2011.040, 2011.

Burkham, D. E.: Channel Changes of the Gila River in Safford Valley, Arizona, 1846–1970, US Government Printing Office, 36 pp., https://pubs.usgs.gov/pp/0655g/report.pdf (last access: 16 May 2022), 1972.

Carlson, B. N., Nittrouer, J. A., Moodie, A. J., Kineke, G. C., Kumpf, L. L., Ma, H., Parsons, D. R., and Wang, H.: Infilling Abandoned Deltaic Distributary Channels Through Landward Sediment Transport, J. Geophys. Res.-Earth, 125, e2019JF005254, https://doi.org/10.1029/2019JF005254, 2020.

Chakraborty, T., Kar, R., Ghosh, P., and Basu, S.: Kosi megafan: Historical records, geomorphology and the recent avulsion of the Kosi River, Quatern. Int., 227, 143–160, https://doi.org/10.1016/j.quaint.2009.12.002, 2010.

Chamberlin, E. P. and Hajek, E. A.: Interpreting Paleo-Avulsion Dynamics from Multistory Sand Bodies, J. Sediment. Res., 85, 82–94, https://doi.org/10.2110/jsr.2015.09, 2015.

Chamberlin, E. P. and Hajek, E. A.: Using bar preservation to constrain reworking in channel-dominated fluvial stratigraphy, Geology, 47, 531–534, https://doi.org/10.1130/G46046.1, 2019.

Chamberlin, E. P., Hajek, E. A., and Trampush, S. M.: Measuring Scales of Autogenic Organization in Fluvial Stratigraphy: An Example from the Cretaceous Lower Williams Fork Formation, Colorado, in: Autogenic Dynamics and Self-Organization in Sedimentary Systems, SEPM Society for Sedimentary Geology, 106, 132–144, https://doi.org/10.2110/sepmsp.106.07, 2016.

Cooper, C. M. and Henry, J. R.: Sediment accumulation and its effects on a Mississippi River oxbow lake, Environ. Geol. Water Sci., 13, 33–37, https://doi.org/10.1007/BF01666569, 1989.

Coulthard, T. J., Macklin, M. G., and Kirkby, M. J.: A cellular model of Holocene upland river basin and alluvial fan evolution, Earth Surf. Proc. Land., 27, 269–288, https://doi.org/10.1002/esp.318, 2002.

Croke, J., Fryirs, K., and Thompson, C.: Channel–floodplain connectivity during an extreme flood event: implications for sediment erosion, deposition, and delivery, Earth Surf. Proc. Land., 38, 1444–1456, https://doi.org/10.1002/esp.3430, 2013.

Edmonds, D. A., Hajek, E. A., Downton, N., and Bryk, A. B.: Avulsion flow-path selection on rivers in foreland basins, Geology, 44, 695–698, https://doi.org/10.1130/G38082.1, 2016.

Edmonds, D. A., Martin, H. K., Valenza, J. M., Henson, R., Weissmann, G. S., Miltenberger, K., Mans, W., Moore, J. R., Slingerland, R. L., Gibling, M. R., Bryk, A. B., and Hajek, E. A.: Rivers in reverse: Upstream-migrating dechannelization and flooding cause avulsions on fluvial fans, Geology, 50, 37–41, https://doi.org/10.1130/G49318.1, 2022.

Ethridge, F. G., Skelly, R. L., and Bristow, C. S.: Avulsion and Crevassing in the Sandy, Braided Niobrara River: Complex Response to Base-Level Rise and Aggradation, in: Fluvial Sedimentology VI, John Wiley & Sons, Ltd, 179–191, https://doi.org/10.1002/9781444304213.ch14, 1999.

Farrell, K. M.: Sedimentology and Facies Architecture of Overbank Deposits of the Mississippi River, False River Region, Louisiana, in: Recent Developments in Fluvial Sedimentology, Special Publication 39, Society of Economic Paleontologists and Mineralogists, 111–120, https://doi.org/10.2110/pec.87.39.0111, 1987.

Gabet, E. J.: Gopher bioturbation: field evidence for non-linear hillslope diffusion, Earth Surf. Proc. Land., 25, 1419–1428, https://doi.org/10.1002/1096-9837(200012)25:13<1419::AID-ESP148>3.0.CO;2-1, 2000.

Gibling, M. R., Bashforth, A. R., Falcon-Lang, H. J., Allen, J. P., and Fielding, C. R.: Log Jams and Flood Sediment Buildup Caused Channel Abandonment and Avulsion in the Pennsylvanian of Atlantic Canada, J. Sediment. Res., 80, 268–287, https://doi.org/10.2110/jsr.2010.024, 2010.

Hack, J. T. and Goodlett, J. C.: Geomorphology and forest ecology of a mountain region in the central Appalachians, Geomorphology and forest ecology of a mountain region in the central Appalachians, United States Government Printing Office, Washington, DC, https://doi.org/10.3133/pp347, 1960.

Hajek, E. A. and Wolinsky, M. A.: Simplified process modeling of river avulsion and alluvial architecture: Connecting models and field data, Sediment. Geol., 257–260, 1–30, https://doi.org/10.1016/j.sedgeo.2011.09.005, 2012.

Hajek, E. A., Heller, P. L., and Sheets, B. A.: Significance of channel-belt clustering in alluvial basins, Geology, 38, 535–538, https://doi.org/10.1130/G30783.1, 2010.

Hartley, A. J., Weissmann, G. S., Nichols, G. J., and Scuderi, L. A.: Fluvial form in modern continental sedimentary basins: Distributive fluvial systems: REPLY, Geology, 38, e231, https://doi.org/10.1130/G31588Y.1, 2010a.

Hartley, A. J., Weissmann, G. S., Nichols, G. J., and Warwick, G. L.: Large Distributive Fluvial Systems: Characteristics, Distribution, and Controls on Development, J. Sediment. Res., 80, 167–183, https://doi.org/10.2110/jsr.2010.016, 2010b.

Harwood, K. and Brown, A. G.: Fluvial processes in a forested anastomosing river: Flood partitioning and changing flow patterns, Earth Surf. Proc. Land., 18, 741–748, https://doi.org/10.1002/esp.3290180808, 1993.

Jahns, R. H.: Geologic features of the Connecticut Valley, Massachusetts, as related to recent floods, USGS, https://doi.org/10.3133/wsp996, 1947.

Jerolmack, D. J.: Conceptual framework for assessing the response of delta channel networks to Holocene sea level rise, Quaternary Sci. Rev., 28, 1786–1800, https://doi.org/10.1016/j.quascirev.2009.02.015, 2009.

Jerolmack, D. J. and Mohrig, D.: Conditions for branching in depositional rivers, Geology, 35, 463–466, https://doi.org/10.1130/G23308A.1, 2007.

Jerolmack, D. J. and Paola, C.: Complexity in a cellular model of river avulsion, Geomorphology, 91, 259–270, https://doi.org/10.1016/j.geomorph.2007.04.022, 2007.

Jones, L. S. and Schumm, S. A.: Causes of Avulsion: An Overview, in: Fluvial Sedimentology VI, John Wiley & Sons, Ltd, 169–178, https://doi.org/10.1002/9781444304213.ch13, 1999.

Khalsa, S. J. S., Borsa, A., Nandigam, V., Phan, M., Lin, K., Crosby, C., Fricker, H., Baru, C., and Lopez, L.: OpenAltimetry – rapid analysis and visualization of Spaceborne altimeter data, Earth Sci. Inform., https://doi.org/10.1007/s12145-020-00520-2, 2020.

Kołaczek, P., Gałka, M., Apolinarska, K., Gębica, P., Superson, S., Michno, A., Harmata, K., Szczepanek, K., Płóciennik, M., Gąsiorowski, M., Karpińska-Kołaczek, M.: Lost in dating – Problems with the absolute chronologies and sedimentation rates of Late Glacial and Early Holocene oxbow lake deposits in Central Europe, Quatern. Geochronol., 41, 187-201, https://doi.org/10.1016/j.quageo.2017.05.002, 2017.

Leeder, M. R.: A Quantitative Stratigraphic Model for Alluvium, with Special Reference to Channel Deposit Density and Interconnectedness, in: Fluvial Sedimentology, Canadian Society of Petroleum Geologists Memoir 5, 587–596, 1977.

Leier, A. L., DeCelles, P. G., and Pelletier, J. D.: Mountains, monsoons, and megafans, Geology, 33, 289–292, https://doi.org/10.1130/G21228.1, 2005.

Lewis, G. W. and Lewin, J.: Alluvial Cutoffs in Wales and the Borderlands, in: Modern and Ancient Fluvial Systems, John Wiley & Sons, Ltd, 145–154, https://doi.org/10.1002/9781444303773.ch11, 1983.

Mackey, S. D. and Bridge, J. S.: Three-dimensional model of alluvial stratigraphy; theory and applications, J. Sediment. Res., 65, 7–31, https://doi.org/10.1306/D42681D5-2B26-11D7-8648000102C1865D, 1995.

Makaske, B., Maathuis, B. H. P., Padovani, C. R., Stolker, C., Mosselman, E., and Jongman, R. H. G.: Upstream and downstream

controls of recent avulsions on the Taquari megafan, Pantanal, south-western Brazil, Earth Surf. Proc. Land., 37, 1313–1326, https://doi.org/10.1002/esp.3278, 2012.

Martin, H. K. and Edmonds, D. A.: harrison-martin/RiverWalk: RiverWalk-AM v1.0.0, Zenodo [code], https://doi.org/10.5281/zenodo.5576789, 2021.

Martin, H. K. and Edmonds, D. A.: Martin and Edmonds Avulsion Model Supplemental Video 1, Supplemental videos of the paper "The push and pull of abandoned channels: How floodplain processes and healing affect avulsion dynamics and alluvial landscape evolution in foreland basins", TIB AV-Portal, https://doi.org/10.5446/54887, 2022a.

Martin, H. K. and Edmonds, D. A.: Martin and Edmonds Avulsion Model Supplemental Video 2, Supplemental videos of the paper "The push and pull of abandoned channels: How floodplain processes and healing affect avulsion dynamics and alluvial landscape evolution in foreland basins", TIB AV-Portal, https://doi.org/10.5446/54888, 2022b.

Martin, H. K. and Edmonds, D. A.: Martin and Edmonds Avulsion Model Supplemental Video 3, Supplemental videos of the paper "The push and pull of abandoned channels: How floodplain processes and healing affect avulsion dynamics and alluvial landscape evolution in foreland basins", TIB AV-Portal, https://doi.org/10.5446/54889, 2022c.

Martin, H. K. and Edmonds, D. A.: Research Data for Martin and Edmonds, 2022, Earth Surface Dynamics, Zenodo [data set], https://doi.org/10.5281/zenodo.6574084, 2022d.

Martin, J., Sheets, B., Paola, C., and Hoyal, D.: Influence of steady base-level rise on channel mobility, shoreline migration, and scaling properties of a cohesive experimental delta, J. Geophys. Res.-Earth, 114, F03017, https://doi.org/10.1029/2008JF001142, 2009.

Mohrig, D., Heller, P. L., Paola, C., and Lyons, W. J.: Interpreting avulsion process from ancient alluvial sequences: Guadalope-Matarranya system (northern Spain) and Wasatch Formation (western Colorado), GSA Bull., 112, 1787–1803, https://doi.org/10.1130/0016-7606(2000)112<1787:IAPFAA>2.0.CO;2, 2000.

Moodie, A. J., Nittrouer, J. A., Ma, H., Carlson, B. N., Chadwick, A. J., Lamb, M. P., and Parker, G.: Modeling Deltaic Lobe-Building Cycles and Channel Avulsions for the Yellow River Delta, China, J. Geophys. Res.-Earth, 124, 2438–2462, https://doi.org/10.1029/2019JF005220, 2019.

Morón, S., Amos, K., Edmonds, D. A., Payenberg, T., Sun, X., and Thyer, M.: Avulsion triggering by El Niño–Southern Oscillation and tectonic forcing: The case of the tropical Magdalena River, Colombia, GSA Bull., 129, 1300–1313, https://doi.org/10.1130/B31580.1, 2017.

Moudrý, V., Lecours, V., Gdulová, K., Gábor, L., Moudrá, L., Kropáček, J., and Wild, J.: On the use of global DEMs in ecological modelling and the accuracy of new bare-earth DEMs, Ecol. Model., 383, 3–9, https://doi.org/10.1016/j.ecolmodel.2018.05.006, 2018.

Nanson, G. C.: Point bar and floodplain formation of the meandering Beatton River, northeastern British Columbia, Canada, Sedimentology, 27, 3–29, https://doi.org/10.1111/j.1365-3091.1980.tb01155.x, 1980.

Nanson, G. C. and Croke, J. C.: A genetic classification of floodplains, Geomorphology, 4, 459–486, https://doi.org/10.1016/0169-555X(92)90039-Q, 1992.

Neuenschwander, A. L. and Pitts, K.: Ice, Cloud, and Land Elevation Satellite 2 (ICESat-2) Algorithm Theoretical Basis Document (ATBD) for Land-Vegetation Along-Track Products (ATL08), https://nsidc.org/sites/nsidc.org/files/technical-references/ICESat2_ATL08_ATBD_r003.pdf TS4, 2020.

Neuenschwander, A. L., Pitts, K., Jelley, B. P., Robbins, J., Klotz, B., Popescu, S. C., Nelson, R. F., Harding, D., Pederson, D., and Sheridan, R.: ATLAS/ICESat-2 L3A Land and Vegetation Height, version 3, NSIDC, https://doi.org/10.5067/ATLAS/ATL08.003, 2020.

O'Loughlin, F. E., Paiva, R. C. D., Durand, M., Alsdorf, D. E., and Bates, P. D.: A multi-sensor approach towards a global vegetation corrected SRTM DEM product, Remote Sens. Environ., 182, 49–59, https://doi.org/10.1016/j.rse.2016.04.018, 2016.

Paola, C., Heller, P. L., and Angevine, C. L.: The large-scale dynamics of grain-size variation in alluvial basins, 1: Theory, Basin Res., 4, 73–90, https://doi.org/10.1111/j.1365-2117.1992.tb00145.x, 1992.

Pelletier, J. D., Mayer, L., Pearthree, P. A., House, P. K., Demsey, K. A., Klawon, J. E., and Vincent, K. R.: An integrated approach to flood hazard assessment on alluvial fans using numerical modeling, field mapping, and remote sensing, GSA Bull., 117, 1167–1180, https://doi.org/10.1130/B25544.1, 2005.

Pizzuto, J. E.: Sediment diffusion during overbank flows, Sedimentology, 34, 301–317, https://doi.org/10.1111/j.1365-3091.1987.tb00779.x, 1987.

Pupim, F. do N., Assine, M. L., and Sawakuchi, A. O.: Late Quaternary Cuiabá megafan, Brazilian Pantanal: Channel patterns and paleoenvironmental changes, Quatern. Int., 438, 108–125, https://doi.org/10.1016/j.quaint.2017.01.013, 2017.

Ratliff, K. M., Hutton, E. H. W., and Murray, A. B.: Exploring Wave and Sea-Level Rise Effects on Delta Morphodynamics With a Coupled River-Ocean Model, J. Geophys. Res.-Earth, 123, 2887–2900, https://doi.org/10.1029/2018JF004757, 2018.

Ratliff, K. M., Hutton, E. W. H., and Murray, A. B.: Modeling long-term delta dynamics reveals persistent geometric river avulsion locations, Earth Planet. Sc. Lett., 559, 116786, https://doi.org/10.1016/j.epsl.2021.116786, 2021.

Reitz, M. D., Jerolmack, D. J., and Swenson, J. B.: Flooding and flow path selection on alluvial fans and deltas, Geophys. Res. Lett., 37, L06401, https://doi.org/10.1029/2009GL041985, 2010.

Richards, K., Brasington, J., and Hughes, F.: Geomorphic dynamics of floodplains: ecological implications and a potential modelling strategy, Freshwater Biol., 47, 559–579, https://doi.org/10.1046/j.1365-2427.2002.00920.x, 2002.

Richardson, P. W., Perron, J. T., and Schurr, N. D.: Influences of climate and life on hillslope sediment transport, Geology, 47, 423–426, https://doi.org/10.1130/G45305.1, 2019.

Rossetti, D. F. and Valeriano, M. M.: Evolution of the lowest amazon basin modeled from the integration of geological and SRTM topographic data, Catena, 70, 253–265, https://doi.org/10.1016/j.catena.2006.08.009, 2007.

Rowland, J. C., Lepper, K., Dietrich, W. E., Wilson, C. J., and Sheldon, R.: Tie channel sedimentation rates, oxbow formation age and channel migration rate from optically stimulated lumines-

cence (OSL) analysis of floodplain deposits, Earth Surf. Proc. Land., 30, 1161–1179, https://doi.org/10.1002/esp.1268, 2005.

Sadler, P. M.: Sediment Accumulation Rates and the Completeness of Stratigraphic Sections, J. Geol., 89, 569–684, https://doi.org/10.1086/628623, 1981.

Schmudde, T. H.: Some Aspects of Land Forms of the Lower Missouri River Floodplain, Ann. Assoc. Am. Geogr., 53, 60–73, 1963.

Schumer, R. and Jerolmack, D. J.: Real and apparent changes in sediment deposition rates through time, J. Geophys. Res.-Earth, 114, F00A06, https://doi.org/10.1029/2009JF001266, 2009.

Slingerland, R. and Kump, L.: Mathematical Modeling of Earth's Dynamical Systems: A Primer, Princeton University Press, 246 pp., ISBN 13 978-0691145143, 2011.

Slingerland, R. and Smith, N.: River avulsions and deposits, Annu. Rev. Earth Planet. Sci., 32, 257–285, https://doi.org/10.1146/annurev.earth.32.101802.120201, 2004.

Smith, N., Slingerland, R., Pérez-Arlucea, M., and Morozova, G.: The 1870s avulsion of the Saskatchewan River, Can. J. Earth Sci., 35, 453–466, https://doi.org/10.1139/cjes-35-4-453, 1998.

Steiger, J., Tabacchi, E., Dufour, S., Corenblit, D., and Peiry, J.-L.: Hydrogeomorphic processes affecting riparian habitat within alluvial channel–floodplain river systems: a review for the temperate zone, River Res. Appl., 21, 719–737, https://doi.org/10.1002/rra.879, 2005.

Sun, T., Paola, C., Parker, G., and Meakin, P.: Fluvial fan deltas: Linking channel processes with large-scale morphodynamics, Water Resour. Res., 38, 26-1–26-10, https://doi.org/10.1029/2001WR000284, 2002.

Toonen, W. H. J., Kleinhans, M. G., and Cohen, K. M.: Sedimentary architecture of abandoned channel fills, Earth Surf. Proc. Land., 37, 459–472, https://doi.org/10.1002/esp.3189, 2012.

Tooth, S., McCarthy, T. S., Brandt, D., Hancox, P. J., and Morris, R.: Geological controls on the formation of alluvial meanders and floodplain wetlands: the example of the Klip River, eastern Free State, South Africa, Earth Surf. Proc. Land., 27, 797–815, https://doi.org/10.1002/esp.353, 2002.

Valenza, J. M., Edmonds, D. A., Hwang, T., and Roy, S.: Downstream changes in river avulsion style are related to channel morphology, Nat. Commun., 11, 2116, https://doi.org/10.1038/s41467-020-15859-9, 2020.

Weissmann, G., Hartley, A., Scuderi, L., Nichols, G., Davidson, S., Owen, A., Atchley, S., Bhattacharyya, P., Chakraborty, T., Ghosh, A., Nordt, L., Michel, L., and Tabor, N.: Prograding distributive fluvial systems: Geomorphic models and ancient examples, SEPM, https://doi.org/10.2110/sepmsp.104.16, 1 January 2013.

Weissmann, G. S., Hartley, A. J., Nichols, G. J., Scuderi, L. A., Olson, M., Buehler, H., and Banteah, R.: Fluvial form in modern continental sedimentary basins: Distributive fluvial systems, Geology, 38, 39–42, https://doi.org/10.1130/G30242.1, 2010.

Weissmann, G. S., Hartley, A. J., Scuderi, L. A., Nichols, G. J., Owen, A., Wright, S., Felicia, A. L., Holland, F., and Anaya, F. M. L.: Fluvial geomorphic elements in modern sedimentary basins and their potential preservation in the rock record: A review, Geomorphology, 250, 187–219, https://doi.org/10.1016/j.geomorph.2015.09.005, 2015.

Wells, N. A. and Dorr, J. A.: A Reconnaissance of Sedimentation on the Kosi Alluvial Fan of India, 14, 1987.

Wolman, M. G. and Eiler, J. P.: Reconnaissance study of erosion and deposition produced by the flood of August 1955 in Connecticut, Transactions American Geophysical Union, 39, 1–14, https://doi.org/10.1029/TR039i001p00001, 1958.

Wolman, M. G. and Leopold, L. B.: River flood plains: Some observations on their formation, River flood plains: Some observations on their formation, US Government Printing Office, Washington, DC, https://doi.org/10.3133/pp282C, 1957.

Wren, D. G., Davidson, G. R., Walker, W. G., and Galicki, S. J.: The evolution of an oxbow lake in the Mississippi alluvial floodplain, J. Soil Water Conserv., 63, 129-135, https://doi.org/10.2489/jswc.63.3.129, 2008.

Zani, H., Assine, M. L., and McGlue, M. M.: Remote sensing analysis of depositional landforms in alluvial settings: Method development application to the Taquari megafan, Pantanal (Brazil), Geomorphology, 161–162, 82–92, https://doi.org/10.1016/j.geomorph.2012.04.003, 2012.

Zwoliński, Z.: Sedimentology and geomorphology of overbank flows on meandering river floodplains, Geomorphology, 4, 367–379, https://doi.org/10.1016/0169-555X(92)90032-J, 1992.

Remarks from the typesetter